

24145694



This is to certify that the

dissertation entitled

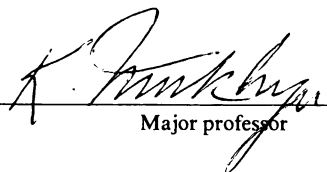
The Effect of Precipitation on Deformation  
and Recrystallization in Cu-5wt.%Ag Alloy

presented by

Wonjoong Kim

has been accepted towards fulfillment  
of the requirements for

Ph.D. degree in Materials Science

  
Major professor

Date May 17, 1990

PLACE IN RETURN BOX to remove this checkout from your record.  
TO AVOID FINES return on or before date due.

DATE DUE	DATE DUE	DATE DUE
_____	_____	_____
_____	_____	_____
_____	_____	_____
_____	_____	_____
_____	_____	_____
_____	_____	_____
_____	_____	_____

MSU Is An Affirmative Action/Equal Opportunity Institution

**THE EFFECT OF PRECIPITATION ON DEFORMATION  
AND RECRYSTALLIZATION IN Cu-5wt%Ag ALLOY**

By

Wonjoong Kim

A DISSERTATION

Submitted to  
Michigan State University  
in partial fulfillment of the requirements  
for the degree of

DOCTOR OF PHILOSOPHY

Department of Metallurgy Mechanics and Materials Science

1990



6059739

## ABSTRACT

### THE EFFECT OF PRECIPITATION ON DEFORMATION AND RECRYSTALLIZATION IN Cu-5wt%Ag ALLOY

By

Wonjoong Kim

The recrystallization texture and microstructural development in heavily rolled supersaturated single phase and aged two phase Cu5%Ag were investigated. The rolling textures of both alloys are of transition type. The two phase alloy revealed a microstructure with elongated fibrous precipitates which was rod shaped before rolling, and its recrystallization texture is a mixed texture comprising retained rolling cube texture. The single phase material recrystallized concurrently with discontinuous precipitation, giving rise to a fibrous microstructure. The precipitates were commonly crystallographically aligned along  $\langle 110 \rangle$ , but not all crystallographically equivalent sets were observed. The recrystallization texture of the supersaturated solid solution was found to be vary according to the annealing temperature but essentially a typical transition type recrystallization texture. A texture randomization during discontinuous precipitation as observed in other system could not be confirmed.

To my family

## TABLE OF CONTENTS

LIST OF TABLES .....	vi
LIST OF FIGURES .....	vii
Chapter 1: INTRODUCTION .....	1
Chapter 2: LITERATURE SURVEY .....	5
Chapter 3: EXPERIMENTAL PROCEDURE .....	18
3.1 Material preparation .....	18
3.2 Specimen Preparation .....	18
3.2.1 Rolling Specimens .....	18
3.2.2 Annealing Specimens .....	22
3.2.3 Optical Microscopy Specimens .....	24
3.2.4 Transmission Electron Microscopy Specimens .....	24
3.3 Tensile Tests .....	25
3.4 Differential Thermal Analysis .....	25
3.5 Texture Determination .....	27
Chapter 4: EXPERIMENTAL RESULTS .....	29
4.1 Rolling Texture .....	29
4.2 Recrystallization Texture .....	29
4.3 Deformation Microstructure .....	34
4.4 Recrystallization Microstructure .....	46

4.5 Hardness .....	59
4.6 Stored Energy Measurements .....	61
4.7 Tensile test .....	61
Chapter 5: DISCUSSIONS .....	68
5.1 Precipitation and Recrystallization .....	68
5.2 texture .....	70
Chapter 6: CONCLUSIONS .....	74
LIST OF REFERENCES .....	76

## LIST OF TABLES

Table No.		Page
2-1	Summary of main characteristics in rolled f.c.c. metals .....	15
3-1	Analyzed chemical composition of experimental alloys .....	19
3-2	Jet polishing conditions for Cu5wt%Ag .....	23
4-1	List of the interplanar spacings of matrix and precipitates .....	52
4-2	Yield limit response data .....	66

## LIST OF FIGURES

Figure 1.1	Schematic TTT diagram for the start of recrystallization and precipitation [2,3]. .....	2
Figure 2.1.	Schematic sketch of combined discontinuous reaction [8]. .....	7
Figure 2.2.	{111} pole figures of rolling textures of Cu and Cu-Zn alloys before and after recrystallization [9]. .....	9
Figure 2.3.	Sections through the plane at $\Phi=90^\circ$ showing probable slip rotations around the cube orientation [16]. .....	10
Figure 2.4.	Changes in the volume fraction of various texture components during recrystallization of cold rolled copper [22]. .....	12
Figure 3.1.	Scheme of specimen preparation .....	20
Figure 3.2.	Vickers hardness as function of temperature for 30 min. isochronal annealing for 90% rolled Cu5%Ag. ....	21
Figure 3.3.	Dimensions of sheet tensile specimen .....	26
Figure 4.1.	Rolling texture of a supersaturated Cu5%Ag. ....	30
Figure 4.2.	Rolling texture of a aged Cu5%Ag. ....	31
Figure 4.3.	Recrystallization texture of a supersaturated Cu5%Ag after annealing at 250° C. ....	32

Figure 4.4. Recrystallization texture of a supersaturated Cu5%Ag after annealing at 450° C. ....	33
Figure 4.5. Recrystallization texture of a aged Cu5%Ag after annealing at 350° C. ....	35
Figure 4.6. Recrystallization texture of a aged Cu5%Ag after annealing at 550° C. ....	36
Figure 4.7. TEM micrograph of a single phase Cu5%Ag before rolling. ....	37
Figure 4.8. Microstructure of a aged two phase Cu5%Ag. ....	38
Figure 4.9. Microstructure of 90% cold rolled single phase Cu5%Ag after annealing at various temperature. ....	40
Figure 4.10. TEM micrographs and diffraction pattern of a single phase Cu5%Ag after 90% rolling. ....	41
Figure 4.11. TEM micrograph and diffraction patterns of a single phase Cu5%Ag showing deformation bands. ....	43
Figure 4.12. Microstructure of 90% cold rolled aged two phase Cu5%Ag after annealing at various temperature. ....	44
Figure 4.13. TEM micrograph aged two phase Cu5%Ag before rolling. ....	45
Figure 4.14. TEM micrographs and diffraction pattern of a single phase Cu5%Ag annealed at	

250° C. ....	47
Figure 4.15. TEM micrographs and diffraction pattern of a single phase Cu5%Ag annealed at 250° C. ....	48
Figure 4.16. TEM micrograph of a single phase alloy after annealing at 250° C. ....	50
Figure 4.17. TEM micrographs and diffraction pattern of a single phase Cu5%Ag annealed at 450° C. ....	51
Figure 4.18. TEM micrograph aged two phase Cu5%Ag annealed at 100° C. ....	53
Figure 4.19. TEM micrographs and diffraction pattern of aged two phase Cu5%Ag annealed at 100° C. ....	55
Figure 4.20. TEM micrograph aged two phase Cu5%Ag annealed at 200° C. ....	56
Figure 4.21. TEM micrograph aged two phase Cu5%Ag annealed at 300° C. ....	57
Figure 4.22. TEM micrographs and diffraction pattern of aged two phase Cu5%Ag annealed at 550° C. ....	58
Figure 4.23. Vickers hardness as function of temperature for 30 min. isochronal annealing for 90% rolled Cu5%Ag. ....	60



Figure 4.24. Stored energy release of a solid solution alloy rolled to 95% reduction. ....	62
Figure 4.25. The engineering stress-strain curve after rolling: (a) solid solution alloy (b) aged two phase alloy. ....	63
Figure 4.26. The engineering stress-strain curve of a solid solution alloy: (a) after rolling (b) after annealing at 250° C. (c) after annealing at 450° C. ....	64
Figure 4.27. The engineering stress-strain curve of a two phase alloy: (a) after rolling (b) after annealing at 350° C. (c) after annealing at 550° C. ....	65

## CHAPTER 1

### INTRODUCTION

The recrystallization behavior of alloys is of primary interest for the processing of commercial materials and thus, has been subject of numerous investigations, which have been reviewed recently [1,2,3,4]. Fundamental contributions to the understanding of the complex and often seemingly contradictory observations are due to Hornbogen and collaborators [2,3], who particularly focussed on the time dependence, and therefore sequence and interaction of the various processes that can occur during the annealing of deformed two phase alloys and supersaturated solid solutions. Their basic approach considers both recrystallization and precipitation as thermally activated processes however with different time constants, such that for the time to start any of these processes

$$t_i = t_{i0} \exp(Q_i/kT) \quad i = R \text{ or } P$$

where  $R$  stands for recrystallization and  $P$  for precipitation.  $Q_P$  depends of course on temperature, because of the existence of an equilibrium temperature for the phase transformation. Hence, in a plot  $1/T$  vs.  $\ln t_i$  (Fig. 1) a straight line is obtained for recrystallization, while the precipitation curve degenerates to a 'nose' close to the equilibrium temperature. The position of both curves relative to each other can be influenced by the degree of deformation. With increasing strain both curves are shifted to smaller times, usually the recrystallization curve more strongly than the precipitation curve. For very high strains the recrystallization curve may not intersect

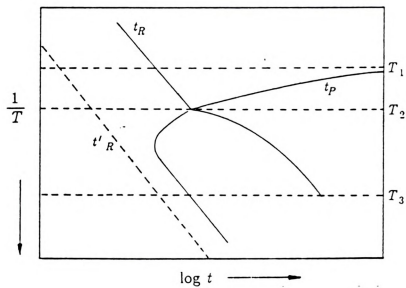


Figure 1.1 Schematic TTT diagram for the start of recrystallization and precipitation [2,3].

the precipitation curve, and recrystallization will begin (or may even go to completion) before precipitation commences. However, in the more usual case recrystallization and precipitation curves will intersect, giving rise to basically four different temperature regimes:

- $T > T_1$  : only recrystallization in a solid solution
- $T_1 > T > T_2$  : precipitation subsequent to recrystallization
- $T_2 > T > T_3$  : interaction of recrystallization and precipitation
- $T_3 > T$  : only precipitation (no recrystallization assumed below  $T_3$ )

The most interesting case is the annealing at  $T < T_2$ . For  $T \ll T_2$  precipitation will be essentially complete before recrystallization starts. This corresponds to recrystallization in a two phase material. If  $T \approx T_2$ , recrystallization and precipitation occur concurrently, but also interactively, commonly referred to as discontinuous precipitation, but a recrystallization process by nature, since the moving grain boundaries remove the deformed structure (dislocations) and simultaneously promote precipitation.

The microstructure due to discontinuous precipitation consists of lamellae and thus, is fundamentally different from aged two phase alloys. This could be exploited for directional reinforcement, if the texture of the recrystallized material would be strongly pronounced. In their investigation on a variety of commercial alloys, Hornbogen and Kreye [2] always noticed a virtually complete randomization of the texture during discontinuous precipitation, even from sharp deformation textures, and they interpreted their results as being due to segregation in the grain boundaries and consequently a loss of growth anisotropy. It is doubtful, though, that this interpretation can be generalized, since many solid solutions of binary systems with limited solubility of both constituents (e.g. Cu30%Zn) develop a very pronounced recrystallization

texture. To address this problem more in detail, the current study focuses on the system Cu-Ag, where adverse segregation effects are anticipated to be less severe.

## CHAPTER 2

### LITERATURE SURVEY

#### 2.1 Recrystallization of Heterogeneous Alloys

It has been shown [5,6] that the velocity  $v$  of the combined discontinuous reaction front for a cold deformed supersaturated alloy can be written as:

$$v = r(F_D + F_C)$$

where  $r$  is the mobility of the reaction front, which involves the boundary diffusion coefficient and the diffusion path.  $F_D$  is the driving force due to the deformed structure, and  $F_C$  is the driving force due to the difference in chemical free energy. Recrystallization of highly deformed metals occurs by creation and motion of grain boundaries. The driving force for primary recrystallization is the elastic stored energy in the strain fields of the dislocations which comprise the deformed structure. The gain in free energy per unit volume swept by the grain boundary and therefore the driving force is given by

$$F_D = 1/2\mu b^2\rho_D$$

where  $\mu$  is the shear modulus,  $b$  is the Burgers vector, and  $\rho_D$  is the dislocation density of the deformed state.

In most cases more than one driving force is effective for the motion of a grain boundary. In addition to the stored energy of cold work, recrystallization of supersaturated solid solutions is affected by precipitation of particles. For an ideal supersaturated solid solution of concentration  $C_o$ , corresponding to the equilibrium temperature  $T_o$ , the chemical driving force at the recrystallization temperature  $T_1$  with equilibrium concentration  $C_1$  can be approximated by the following equation:

$$F_C = k/\Omega(T_1 - T_o)C_o \ln C_o$$

where  $\Omega$  is the atomic volume, and  $k$  the Boltzmann constant. If  $F_C$  is the only driving force, the process is known as discontinuous precipitation. When  $F_D$  and  $F_C$  are effective at the same time, the process is known as the combined discontinuous reaction.

The retarding force due to the pinning of a grain boundary by precipitates acts against the driving forces. Zener referred to by Smith [7] developed the equation for the interaction force between a boundary and a particle:

$$F_P = \frac{3f\gamma}{2r}$$

where  $f$  is the volume fraction,  $r$  the radius of the particles and  $\gamma$  is the specific energy of the grain boundary. In the case  $F_D + F_C > F_P$ , combined discontinuous reaction occurs as shown in Fig. 2-1. If  $F_D + F_C < F_P$ , recrystallization proceeds without any motion of large angle grain boundaries (continuous recrystallization). Hornbogen [8] described the microscopic process by subgrain coalescence or Y-node motion.

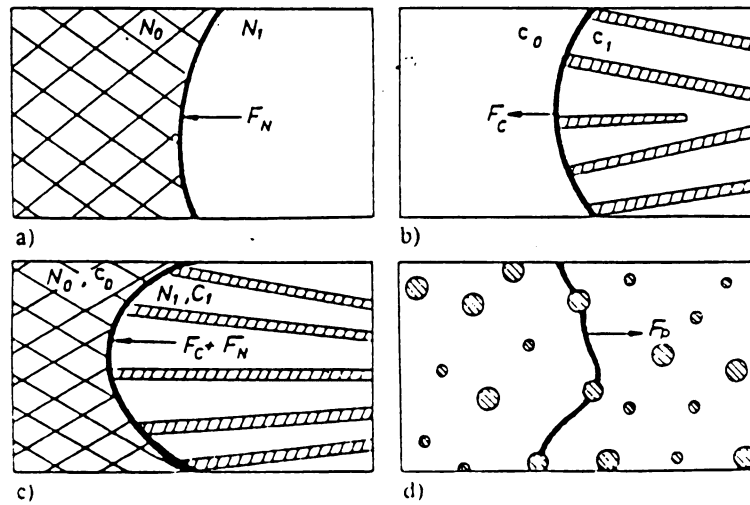


Figure 2.1. Schematic sketch of combined discontinuous reaction [8].



## 2.2 Textures

There are two basic types of deformation and corresponding recrystallization textures as shown in Fig. 2-2. During room temperature rolling the copper type texture occurs in metals with a stacking fault energy higher than  $\sim 40\text{mJ/m}^2$ , while the brass type texture develops in alloys with a stacking fault energy lower than  $\sim 20\text{mJ/m}^2$ . Textures in rolled sheets can be usually described by a few ideal orientations in terms of the plane  $\{hkl\}$  that lies parallel to the plane of the sheet and the direction  $[uvw]$  that is parallel to the rolling direction. The copper type rolling texture can be expressed by  $\{112\}\langle 111\rangle$ ,  $\{123\}\langle 634\rangle$  and  $\{011\}\langle 211\rangle$  components while the brass type rolling texture is characterized by  $\{110\}\langle 112\rangle$  plus  $\{110\}\langle 001\rangle$  components. On recrystallization the copper type rolling texture changes into the cube texture and the brass type rolling texture leads to the brass type recrystallization containing  $\{326\}\langle 835\rangle$  as the main orientation. The transition between the two types of rolling texture has been studied in various copper alloys [9-13]. The transition from the copper type to the brass type texture can be inferred by decreasing the temperature of rolling or by increasing of the solute content at constant rolling temperature. This has been shown in copper alloys [14]. An increasing tendency for mechanical twinning during deformation is the mechanism which causes the f.c.c. rolling texture transition with decreasing stacking fault energy [15].

In alloys, two types of recrystallization textures may result from the copper type rolling texture, namely the cube texture and the retained rolling texture. The influence of second phase particles and alloying elements is important for the corresponding recrystallization texture. Dillamore and Katoh [16] developed a model of texture formation of f.c.c./b.c.c. alloys which predicts the existence of transition bands in which a central region of the curved lattice contains the cube orientation. Fig. 2-3 demonstrates that certain crystals will tend to approach the cube orientation by

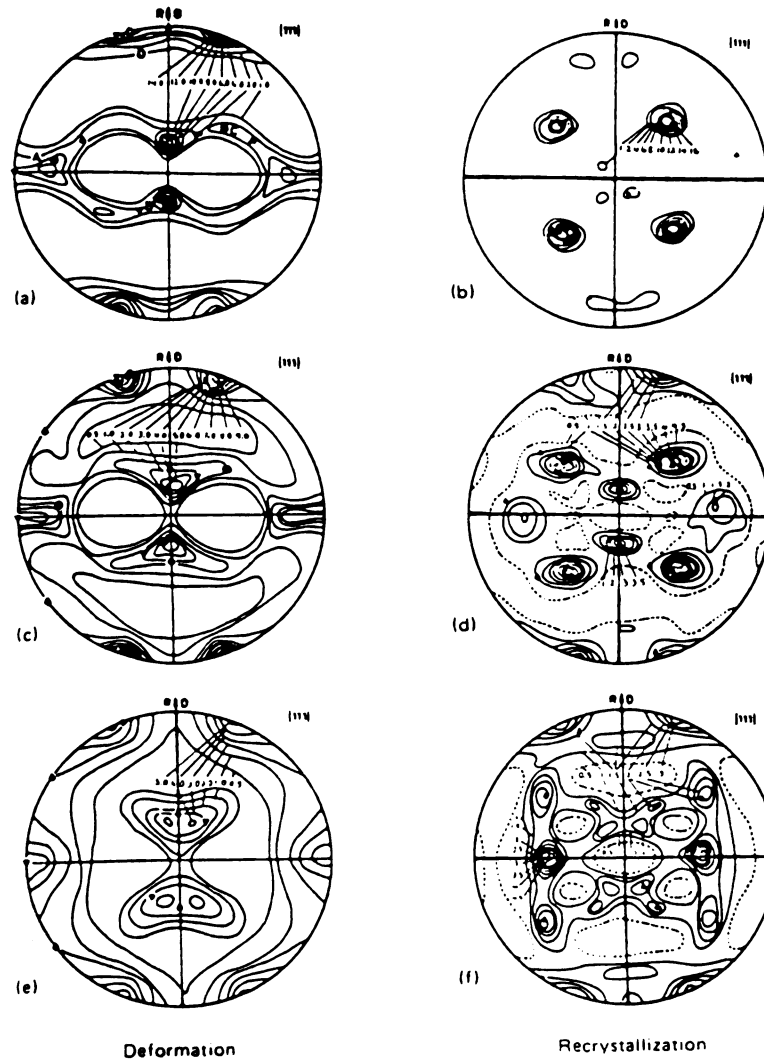


Figure 2.2.  $\{111\}$  pole figures of rolling textures of Cu and Cu-Zn alloys before and after recrystallization [9].

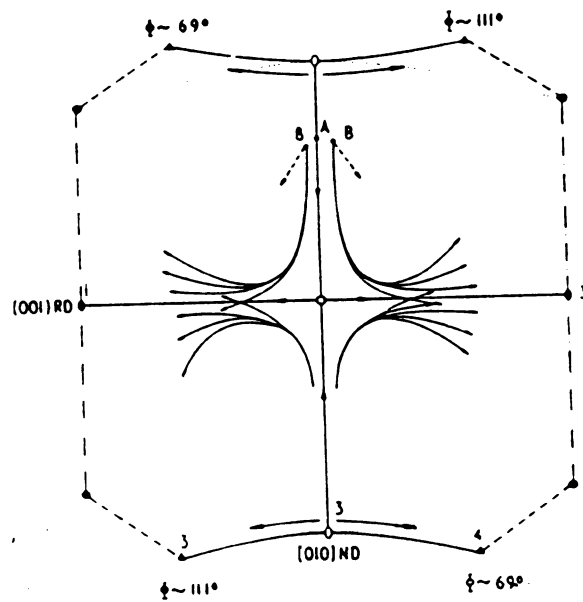


Figure 2.3. Sections through the plane at  $\Phi=90^\circ$  showing probable slip rotations around the cube orientation [16].

rotation around the normal direction and then subsequently diverge by rotation around the rolling direction, eventually arriving at one of the stable orientations. The cube orientation was actually found in the deformed microstructure of copper by electron microscopic investigations [17,18]. These nuclei may occur either as dynamically recovered subgrains [17] or highly elongated microbands [18] which recover statically at a very early stage of annealing. This was explained by Ridha and Hutchinson as a unique dislocation symmetry of the cube orientation which favours recovery in these areas compared to the other orientations. The nucleation mechanism involved is subgrain growth, which occurs by bulging of the microband boundaries. Ridha and Hutchinson showed this nucleation mechanism using lightly annealed pure copper in which a cube oriented deformation structure is present and is bowing out along one side as a series of mini bulges into the adjacent substructure. Many observations show that this is the typical pattern of behavior. At a slightly later stage the small bulges link together producing a continuous front which advances into the neighbouring dislocated substructure. They found that the nuclei of cube orientation are located in transition bands. The cube orientation is known to occur at the early stage of recrystallization process [19]. The origin of cube texture has been studied recently by many authors [18,20,21]. Virnich et al. [33] followed the progress of recrystallization in cold rolled copper using quantitative texture measurements. Their results ( Fig. 2-4) show that the cube component first increases at the expense of the copper component  $\{211\}\langle 111 \rangle$ . The S component  $\{123\}\langle 634 \rangle$  is consumed later and both these components continue to diminish subsequently at a stage where the rate of development of the cube texture is greatly reduced.

The formation of recrystallization textures can be explained by either oriented growth or oriented nucleation. The theory of oriented growth is based on the observation of the orientation dependence of grain boundary migration in single crystals. Measurements of grain boundary movement in deformed aluminum and copper single

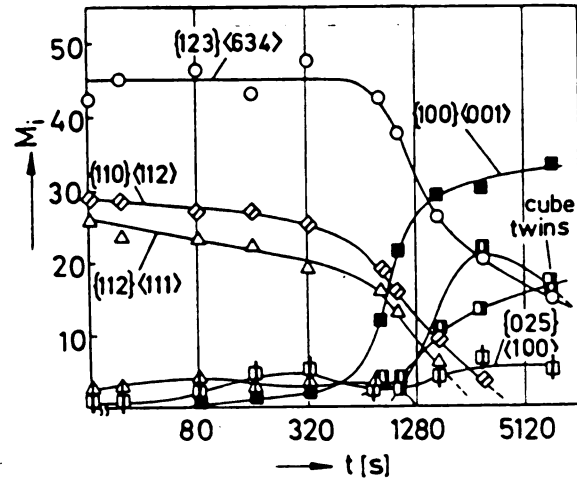


Figure 2.4. Changes in the volume fraction of various texture components during recrystallization of cold rolled copper [22].

crystals [23-25] have revealed that boundaries between crystals with a common  $\langle 111 \rangle$  axis and an orientation relationship described by a  $30^\circ$  or  $40^\circ$  rotation around this axis move the fastest. According to this theory all kinds of orientations are nucleated and the nuclei which have a favorable orientation relationship with the deformed matrix determine the recrystallization texture. In polycrystalline materials the orientation relationship between the nuclei and its neighbors are more complicated. It has to be considered that the grains have to grow into several orientations corresponding to the different component of the deformation texture. The recrystallization texture formed by such a process is called a compromise texture. The brass recrystallization texture is the typical example of a compromise texture. According to the theory of oriented nucleation formulated by Burgers et al. [26] the formation of recrystallization textures is governed by the nucleation process. They proposed crystallites which are present within the deformed structure and which are cube oriented undergo recovery faster than those of other orientations. Cube oriented nuclei produced by rapid polygonization can subsequently grow by large angle grain boundary migration.

### 2.3 Microstructure of the Deformed State

Since a recrystallization texture is determined by the structure formed during deformation, nucleation from the deformed state is of major interest in recrystallization textures. In heavily deformed metals nucleation initiates in band shaped inhomogeneities such as deformation bands, shear bands and kink bands [27]. At higher degrees of deformation, the microstructure consists of elongated cells. If the cell have small orientation difference across the boundary [28]. Clusters of these bands are sometimes etched at higher strains as characteristic markings in the optical microstructure. Deformation bands are regions with a uniform orientation having a band like

structure usually lying parallel to the deformation direction. The structure between two deformation bands is called a transition band. Since the orientation changes gradually but continuously from one side of a transition band to the other, large orientation differences up to  $30^\circ$  can be built up. Shear bands [29] are reported to form at angles of about  $35^\circ$  to the rolling direction (Fig. 2-5) and cut through differently oriented regions without significant deviation. Even though the bands have quite different orientations from their neighbors, the copper type deformation texture is not affected by them [30]. The heterogeneities in the microstructure described above have been observed to be nucleation sites for primary recrystallization. The main characteristic features of the heterogeneous microstructure in f.c.c. metals and alloys are summarized in Table 2-1 [11].

The important mechanisms of nucleation are strain induced grain boundary migration or bulging, and the processes of subgrain formation and subgrain enlargement by the migration or elimination, respectively, of small angle boundaries. The features of subgrain enlargement can be similar to either normal grain growth or secondary recrystallization. The kinetics of these processes can be the basis for the subgrain enlargement observed in materials containing second phase particles. If particles of a second phase exist, nucleation of primary recrystallization can be accelerated or retarded. The effect of second phase particles is determined by both their size and volume fraction. If coarse particles are present before deformation, the region around them can be a favourable nucleation site since a large orientation gradient and deformation develop in that area [31]. If very fine particles are present, the dislocation structure is uniform [32]. Precipitation shortly before recovery has a similar effect. Here the major process is subgrain enlargement which is dependent on particle growth which is recrystallization in situ.

	SFE		
Strain	High	Medium	Low
Low	Grain elongation Deformation bands Equixed cells	Grain elongation Deformation bands Equixed cells Microbands	Grain elongation Deformation bands Stacking faults Deformation twins
Medium	As above	As above Some clustering and alignment of microbands	As above Some alignment of twins Shear bands at higher strains
High	As above	As for 1 Extensive microband alignment and clustering Shear bands	As for 1 Twin alignment Continuing replacement of twinned structure by shear bands

Table 2-1 Summary of main characteristics in rolled f.c.c. metals



## 2.4 Precipitation

Precipitation from a supersaturated solid solution can proceed by the spinodal decomposition or by the nucleation and growth mechanisms. In the spinodal process no interface effects are involved, but for the nucleation and growth process the formation and motion of an interface are the essential features of the transformation. The classical theory of the nucleation process[33,34] requires that the nucleus forms with the minimum possible value of surface energy per unit volume of precipitate. For a precipitate with isotropic interfacial energy, this requires a spherical nucleus shape by the Gibbs Wulff theorem [33,35]. However, of usual case in the solid state precipitation where the two phases have different crystal structures, a low energy interface occurs only for particular well matched planes or directions [35,36]. This constraint favors the particular relative orientation relationships between the two phases namely those that give good matching. Nucleation can also occur heterogeneously on dislocations [37,38]. A special case is the situation where the nucleus and the matrix have the same crystal structure and similar lattice parameter and are found in the so called 'cube-cube' identical orientation relationship. In this case a low interfacial energy is expected, showing almost no variation with interface orientation, and giving a nearly spherical equilibrium shape as observed [39].

The migration of a large angle grain boundary can pass through a set of precipitates during recrystallization and grain growth. If the precipitates in the consumed matrix grain are coherent with the matrix, then a range of interesting interactions may occur. Many investigations have been made into this process for the case where both phases have the same crystal structure. The following phenomena have been commonly reported:

- 1) The grain boundary does not pass through the precipitates, which therefore retain their initial orientation and become incoherent after recrystallization [40].
- 2) The coherent precipitates dissolve after contact with the moving grain boundary and precipitate coherently with the new grain, either discontinuously at the moving grain boundary or continuously at some distance behind the grain boundary. Both cases have been observed experimentally [41,42,43].
- 3) The grain boundary is held by the coherent precipitates which then coarsen, leading to a complete halt of the boundary movement. With additional nucleation of recrystallization the so-called 'necklace structure' of new grains forms [44,45,46]. This is a network of the recrystallized grains along the prior grain boundaries.
- 4) The grain boundary could pass through the coherent precipitate so that both phases suffer the same change of orientation and thereby retain the coherent low energy interface between the two phases [47].

It has frequently been observed that small increases ( about 10% ) in the yield strength of cold worked 70-30 brass are obtained when it is heated at a temperature below the recrystallization temperature. Small but significant hardness increases have been reported by Mohan et al. [48] when cold worked Cu-Zn, Cu-Al, and Cu-Si alloys were heated for about 30 min. at 200° C. It has been generally proposed that the two most probable causes of low temperature hardening of these alloys are short range order [49] and Suzuki locking [50].

## CHAPTER 3

### EXPERIMENTAL PROCEDURE

#### 3.1 Material Preparation

The present experiments were carried out on Cu-5 wt%Ag alloys. To form the alloys Cu and Ag of 99.995% purity were melted in an induction furnace with an argon atmosphere containing 10% hydrogen. For homogenization the alloys were annealed in a vacuum furnace at 850°C for 72h. From this block specimens with 15x10 mm<sup>2</sup> rectangular cross section and 20mm length were machined and rolled to 50% reduction. Then these alloys were solutionized for 7h at 850°C ( in air, wrapped in Cu foil ) and water quenched subsequent to solutionization.

After solution treatment the alloys were chemically analyzed using a nondestructive X-ray microanalysis technique. Analysis was performed in a JEOL JSM 35C SEM which has an analysis unit which adopts the ZAF method. Cu and Ag of 99.995% purity were used as standards and the alloys were used as specimens. Their chemical analyses are given in Table 3-1.

#### 3.2 Specimen Preparation

##### 3.2.1 Rolling Specimens

Two types of rolling samples were prepared as schematically indicated in Fig. 3-1. One set of samples was rolled as quenched, i.e as a supersaturated solid solution (solubility limit at room temperature <1%, at 780°C 7.9%). Another set of samples was annealed for 3 h at 600°C and then water quenched. Since the solubility

Area #	Composition, Wt. Pct.	
	Copper	Silver
1	94.49	5.51
2	94.76	5.24
3	94.73	5.27
4	94.32	5.68
5	94.71	5.29
6	94.50	5.50

Table 3.1. Analyzed Chemical Composition of  
Experimental Alloys

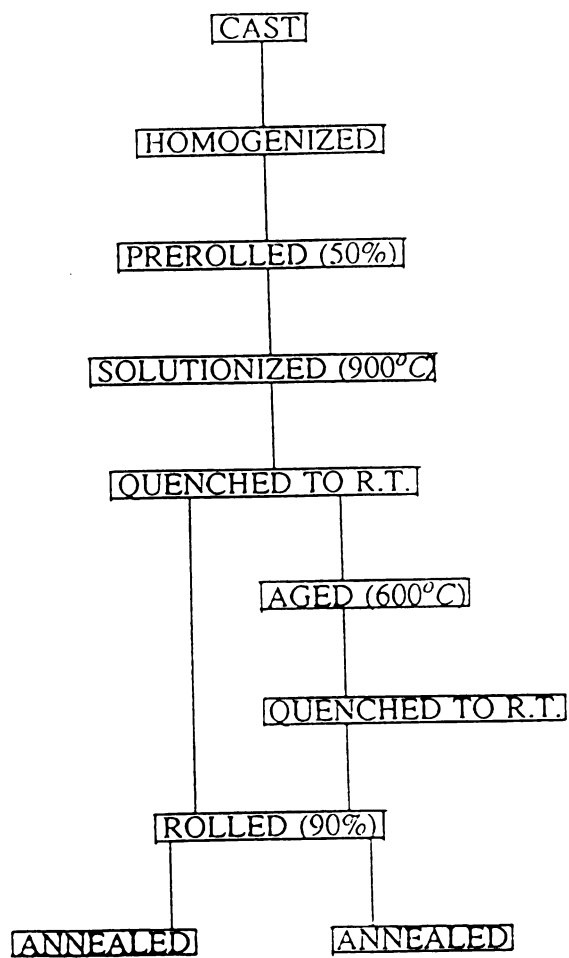


Figure 3.1. Scheme of specimen preparation

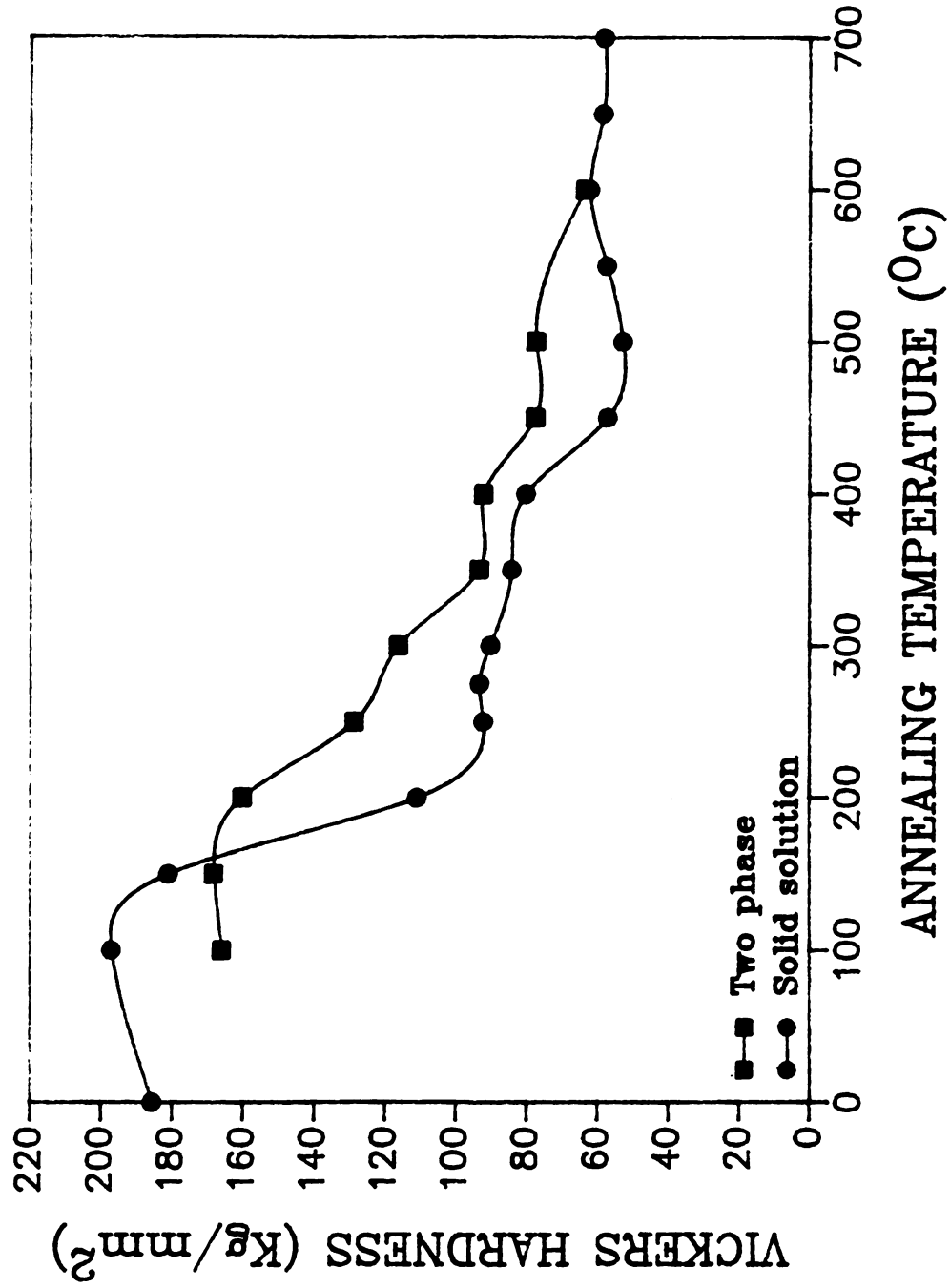


Figure 3.2. Vickers hardness as function of temperature for 30 min. isochronal annealing for 90% rolled Cu5%Ag.

limit at  $600^{\circ}\text{C}$  is 3%, this second type of samples contained precipitates of a silver rich solid solution as was confirmed by TEM (ch. 4). All samples were rolled to a total thickness reduction of 95%. The sample thickness after rolling was  $.5\text{mm}$ . Special care was taken to ensure homogeneous deformation throughout the thickness by keeping the ratio  $l_d/d > 1$  ( $l_d$  - contact length,  $d$  - specimen thickness) [56]. The specimens were turned end for end between passes. To remove any contamination introduced during rolling, the specimens were subsequently thinned by mechanical polishing to  $0.4\text{mm}$  thickness.

### 3.2.2 Annealing Specimens

To establish the recrystallization temperature for the rolled material, specimens of both types were subjected to 30 min isochronal annealing between  $100^{\circ}\text{C}$  and  $700^{\circ}\text{C}$ . The Vickers hardness number was obtained using the microhardness tester (Buehler Micromet) after each annealing treatment. The applied load in the test was 0.3kg: The loading speed was  $50\mu\text{m}/\text{sec}$  and the loading time was 10 seconds. A significant decrease in hardness, which can be attributed to recrystallization, was observed between  $250^{\circ}\text{C}$  and  $300^{\circ}\text{C}$  for the single phase material and between  $350^{\circ}\text{C}$  and  $400^{\circ}\text{C}$  for the two phase material (Fig. 3-2). No pronounced recovery was observed prior to recrystallization. Corresponding to these results, the rolled two phase samples were then subjected to recrystallization annealing for 30 min at  $350^{\circ}\text{C}$  in order to study the influence of the annealing temperature on texture and microstructure. There were two sets of the rolled single phase material. One set was recrystallized for 30 min at  $250^{\circ}\text{C}$  and one set was recrystallized for 30 min at  $450^{\circ}\text{C}$ .

Electrolyte (D2)	Temp ( $^{\circ}$ C)	Voltage (V)	Current (mA)
Distilled Water	14	6	90
phosphoric acid	250ml		
ethanol	250ml		
Vogel's sparbeize	2ml		
propanol	50ml		
urea	5g		

Table 3.2 Jet polishing conditions for Cu5wt. %Ag



### 3.2.3 Optical Microscopy Specimens

Specimens were prepared from longitudinal sections i.e. with the plane of observation containing the rolling plane normal and rolling directions of the rolled sample. The longitudinal sections ND-RD were cut with a Buehler diamond wheel saw. The microstructure was investigated on the cut face of the sample. Specimens were mounted in lucite after slicing and mechanically ground with abrasive grit papers of 240 grit to 600 grit and polished on a cloth, using alumina powder of the size from  $5\mu\text{m}$  to  $0.3\mu\text{m}$  particles to get a scratch free surface. The following etchants were used after polishing.

hydrochloric acid	167ml
water	333ml
iron chloride	25g

Microscopy was performed in a Neophot 21 Microscope.

### 3.2.4 Transmission Electron Microscopy Specimens

Slices about 3mm thick were cut from longitudinal sections (i.e. the plane containing the rolling plane normal and rolling directions) using a Buehler diamond wheel saw. These slices were handground on 600 grit Emery paper to  $100\mu\text{m}$  thick. The final thinning with a Tenupol jet polisher produced thin enough ( $100\text{nm}$ ) specimens. The polishing conditions are given in Table 3-2

In some cases where the electropolishing was not successful, an ion beam thinning technique was used. Argon was used as the bombarding species. The transmission electron microscopy studies were carried out by means of a 200KV Hitachi H800 microscope.

### 3.3 Tensile Tests

Mechanical property data (U.T.S., 0.2 pct. offset Y.S. and elongation ) were determined using an SFM Smart-1 Testing System. Specimens of both single and two phase alloys were tested after 90% cold reduction and after 30 min heat treatments in the range of 250°C to 550°C. All heat treatments were carried out in a vacuum furnace. Suitable tensile specimens were machined from the rolled and annealed sheet and pulled to fracture at room temperature in an United Tensile Tester at a strain rate of 0.0048 in. per in. per min. The specimen dimensions are shown in Fig. 3-3. The tensile specimen was oriented such that its tensile axis was parallel to the direction of rolling. The yield stress was taken as the stress measured at 0.2 pct strain.

### 3.4 Differential Thermal Analysis

Differential thermal analysis (D.T.A.) was performed using a Dupont 900 Differential Thermal Analyzer equipped with a differential scanning calorimeter (D.S.C.) cell. The sample was a solid solution alloy which was rolled to 95% reduction and prepared as a 7.4mg cube. An empty copper pan was used as a reference. Both sample and standard were cleaned ultrasonically with acetone prior to thermal analysis to provide a clean flat surface for contact with the D.S.C cell thermocouples and to avoid surface contamination. The specimen was heated with a rate of 5°C/min. to 650°C under a 90% nitrogen plus 10% hydrogen atmosphere.

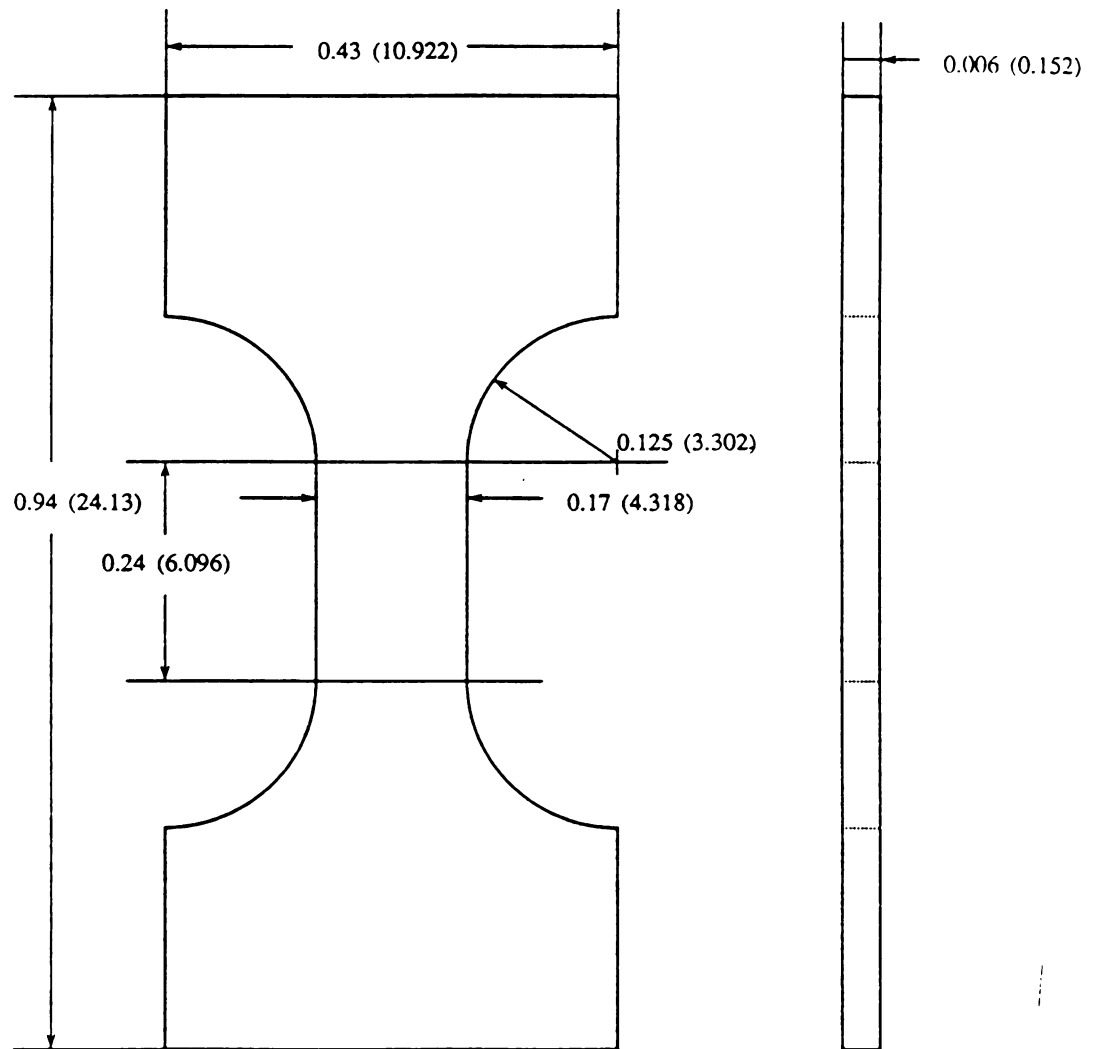


Figure 3.3. Dimensions of sheet tensile specimen

### 3.5 Texture Determination

The crystallographic orientation of an individual crystallite in a polycrystalline sample is defined by the orientation of its crystal coordinate system  $K_c$  with respect to the sample coordinate system  $K_s$ . The orientation  $g$  of  $K_c$  with respect to  $K_s$  can be described by the angles  $\alpha$  and  $\beta$  of a direction  $[uvw]$  and the rotation angle  $\gamma[uvw]$ . If the direction  $[uvw]$  is normal to the reflecting lattice plane  $(hkl)$  then the reflected intensity is independent of a rotation of the crystal through angle  $\gamma$ . Thus polycrystal diffraction yields the orientation distribution of the crystal direction  $[uvw]$  as a function of  $\alpha$  and  $\beta$ . This is called a  $(hkl)$  pole figure.

A Norelco wide range goniometer was mounted on a diffractometer base. An IBM XT computer was adapted to the counter electronics through an OMEGA WB-A10-B Analog-to digital converter for the automatic determination of pole figures.

In order to check the accuracy of this system, an aluminum single crystal and lithium fluoride single crystal were used as the test material. The orientation of the single crystal were verified by Laue patterns.

Usually it is not possible to exactly orient the specimen and thus, to indicate the rolling direction in the pole figure. Thus the rolling direction on the measured pole figure is not in a correct position. It is more accurate to determine the rolling direction by symmetry considerations from the pole figure measurements themselves. This is achieved by rotating the pole figure through an appropriate angle, until the correctly adjusted symmetric pole figure is obtained.

The calculation of the correction factors (i.e. geometrical factor, defocusing factor, and absorption factor) can be avoided if the reflected intensity is compared with the corresponding intensity reflected from a random sample under the same conditions.

The software system can be divided into three parts. The first is used for data acquisition. The second is the pole figure plotting routine. The third part, which is the plot of the ideal orientation, is applied to the second part to figure out components of the pole figure.

The measured intensity data from the data acquisition program are not yet pole density values. The calculation of the correction factor can be avoided if the reflected intensity is compared with the corresponding intensity reflected from a random sample under the same condition. In order to obtain the pole density, corrections have to be applied which are carried out by the normalized pole figure program. This normalization was done by the large number of randomly oriented grains, i.e. a powder sample and expressed as times random. The average intensity of the powder sample is calculated in each step of  $\alpha$  motion and the measured intensity is divided by this value. The final step of the measuring process is the data output or data storage. After the measurement the representation of the data is made by drawing a pole figure on the printer. The pole figure is represented by contour lines of equal intensity level.

## CHAPTER 4

### EXPERIMENTAL RESULTS

#### 4.1 Rolling Texture

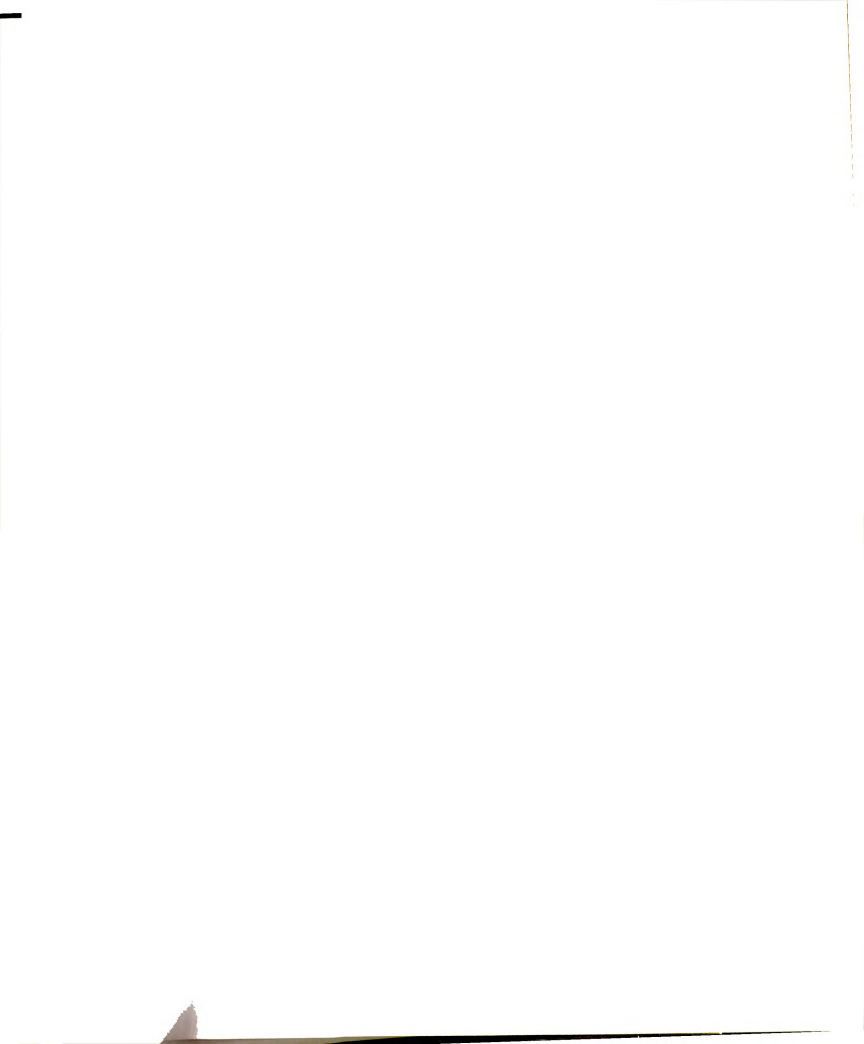
After rolling the texture of the samples was determined by pole figure measurements, using the Schultz reflection method on a Norelco pole figure goniometer with spiral scanning. The data were normalized with regard to a powder specimen of pure Cu.

Rolling textures of aged and supersaturated samples are represented by  $\{111\}$  and  $\{200\}$  pole figures as shown in Fig. 4-1,2. The solid solution alloy rolled to 95% reduction exhibits a transition type rolling texture consisting of S orientation  $\{123\}\langle 634 \rangle$ , brass orientation  $\{011\}\langle 211 \rangle$ , and Goss orientation  $\{011\}\langle 100 \rangle$ . These three texture components are clearly present in both  $\{111\}$  and  $\{200\}$  pole figures.

The two phase alloy rolled to 95% reduction shows essentially the same texture consisting of brass orientation, Goss orientation, and also with intensity close to the S orientation. There was no evidence to distinguish the rolling texture of the solid solution alloy from that of two phase alloy except the split of the highest intensity in between  $\{011\}\langle 211 \rangle$  and  $\{011\}\langle 100 \rangle$  in the  $\{111\}$  pole figure of the solid solution alloy.

#### 4.2 Recrystallization Texture

The recrystallization textures of the solid solution alloy after rolling and annealing at 250° C and 450° C respectively are shown in Fig. 4-3,4. The main components



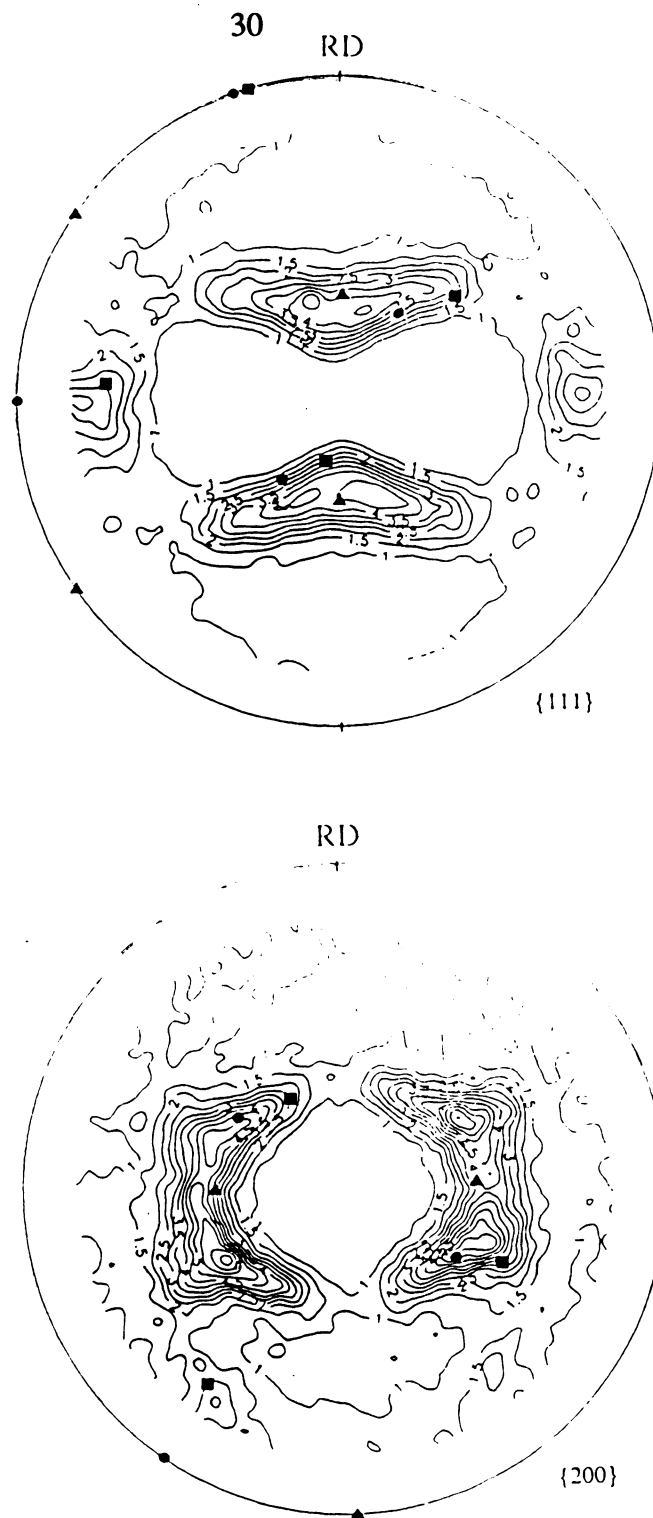


Figure 4.1. Rolling texture of a supersaturated Cu5%Ag.



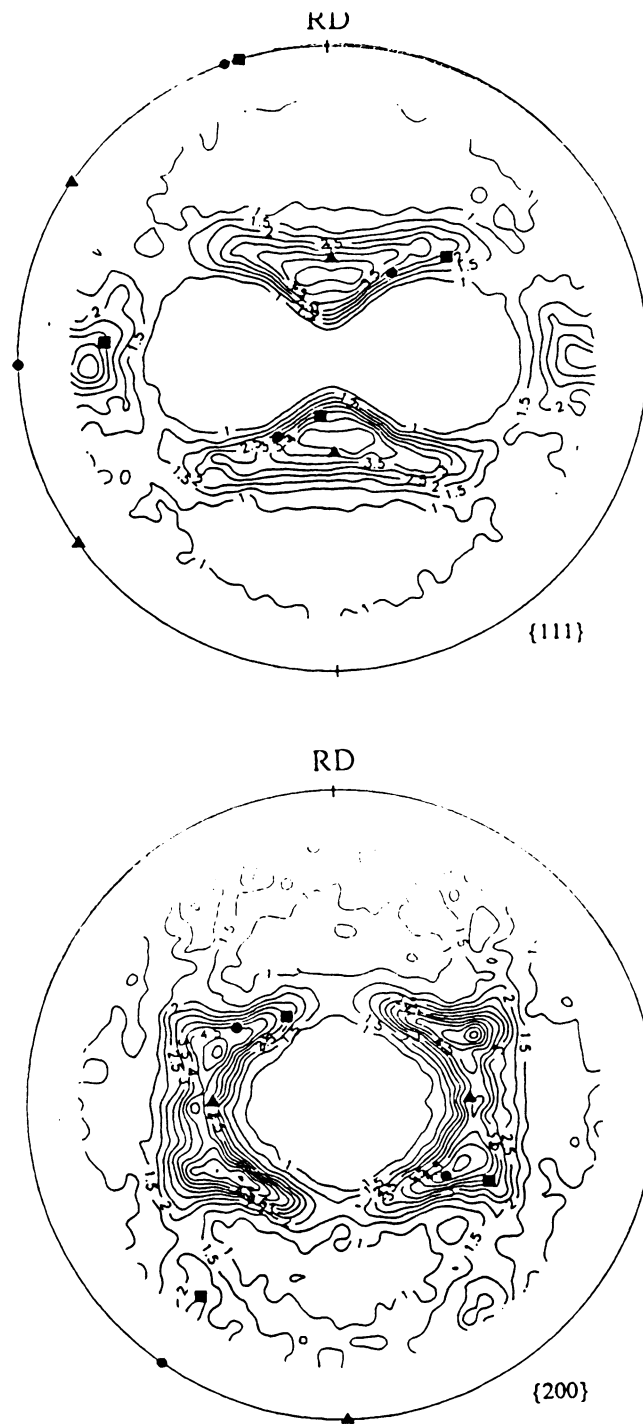


Figure 4.2. Rolling texture of a aged Cu5%Ag.



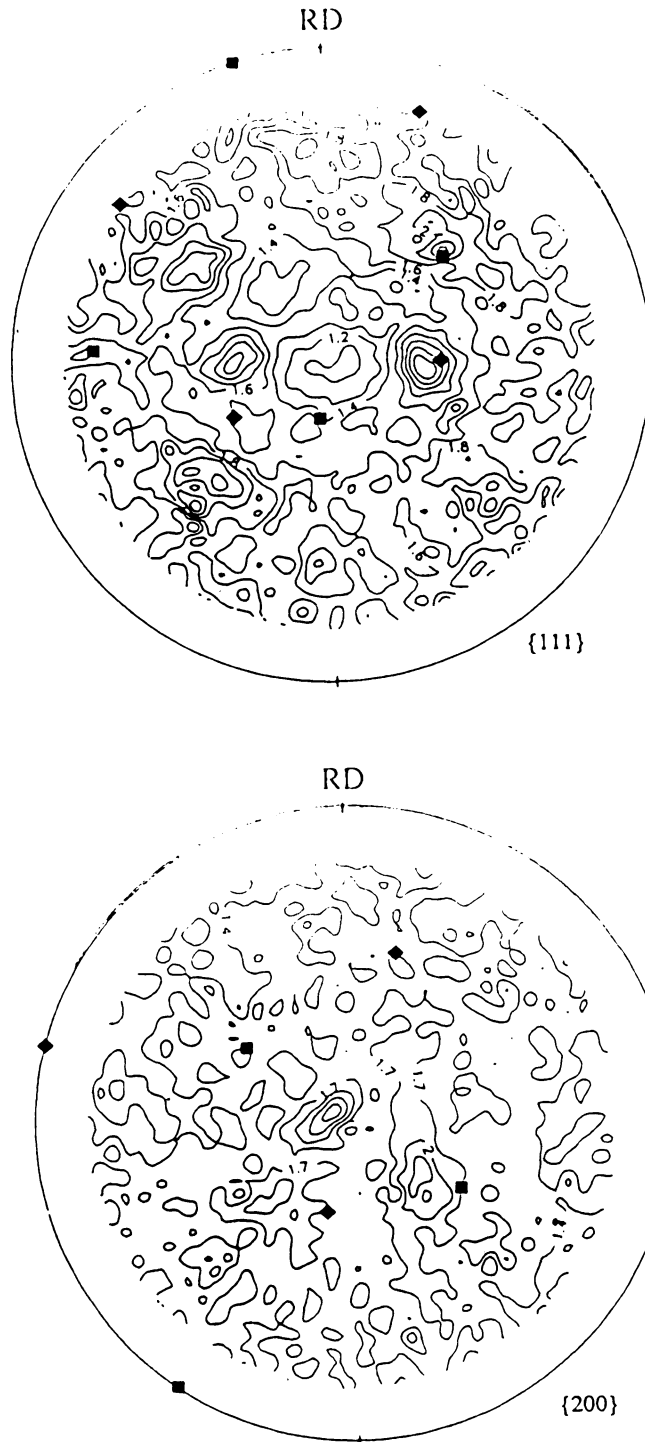


Figure 4.3. Recrystallization texture of a supersaturated Cu5%Ag after annealing at 250° C.

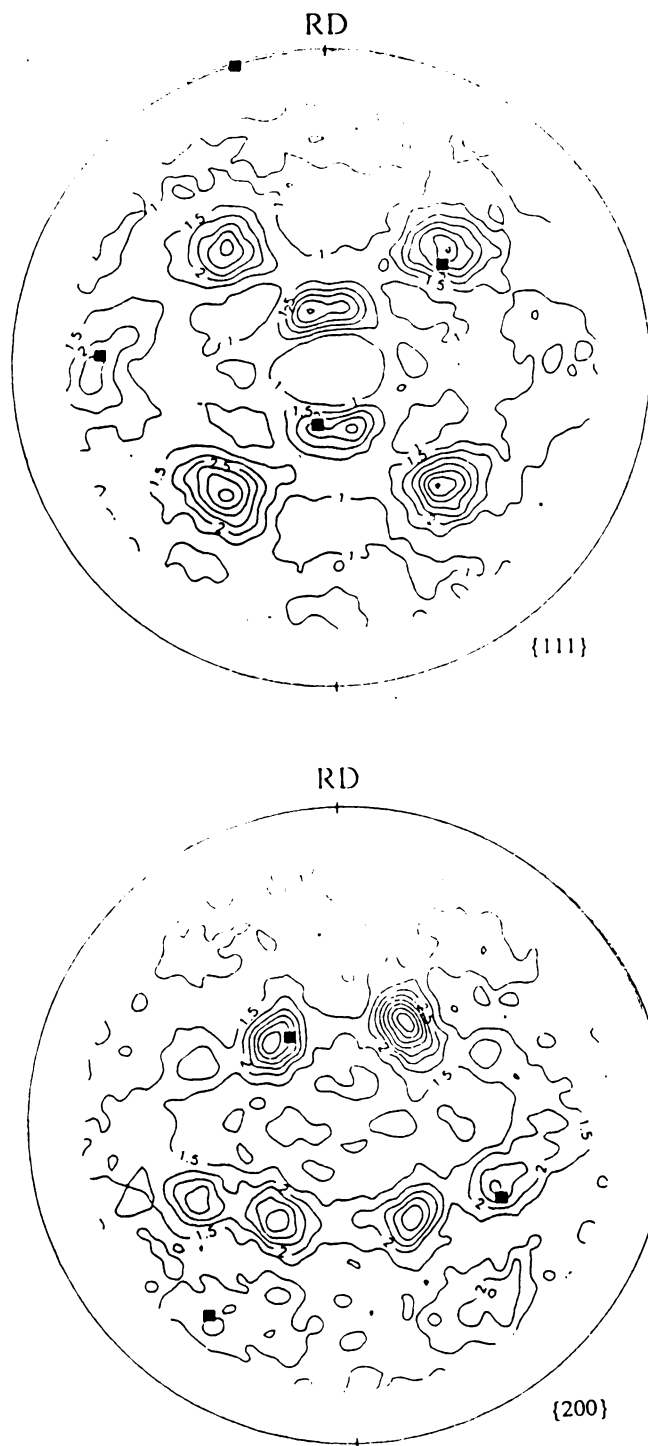


Figure 4.4. Recrystallization texture of a supersaturated Cu5%Ag after annealing at 450°C.

of the specimen annealed at 250° C are {001}<100> and {132}<113>. The recrystallization textures of annealing at 450° C are different from those of annealing at 250° C. While cube orientation {001}<100> exists again, a {368}<423> orientation appears instead of the {132}<113> component.

The recrystallization of the two phase material results in a texture distinctly different from the deformation texture for both annealing at 350° C and 550° C as shown in Fig. 4-5,6. The recrystallization texture for 350° C annealed specimen consists of two components which are {001}<100> and {123}<634>. The recrystallization texture for the 550° C annealed specimen shows essentially the same texture as annealing at 350° C. By comparison of these two recrystallization textures it can be noted that texture is getting sharper as annealing temperature increases.

#### 4.3 Deformation Microstructure

The microstructural development of the deformed single and two phase alloys was investigated through the optical microscope and especially the electron microscope. The microstructure of the supersaturated solid solution alloy prior to deformation was investigated to assure the attainment of a homogeneous solid solution. The electron micrographs shown in Fig. 4-7. reveal that the microstructure is not actually homogeneous. Instead these are needles of submicron size as straight lines or spots depending on their orientation with respect to the angle of observation. The existence of these precipitates may be due to an imperfect quenching procedure or precipitation at room temperature after quenching. The former case is more likely than the latter case, since in general the rate of precipitation from a copper based supersaturated solid solution is very slow.

The microstructure of a two phase alloy which was precipitation treated at 600° C for 3 hours to purposely obtain a second phase is given in Fig. 4-8. As

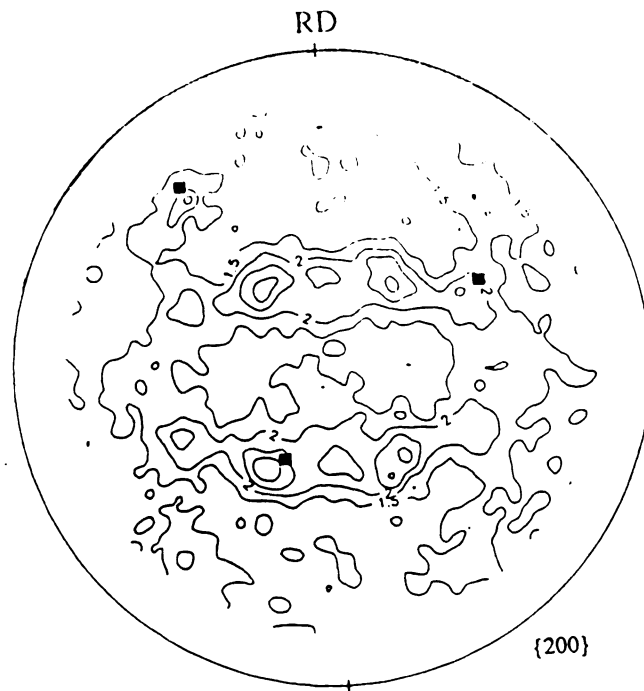
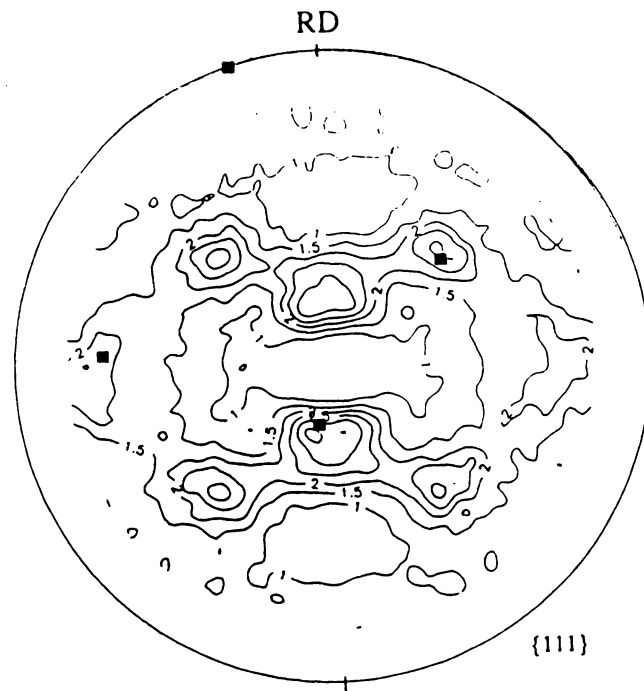


**Figure 4.5. Recrystallization texture of a aged Cu5%Ag after annealing at 350° C.**

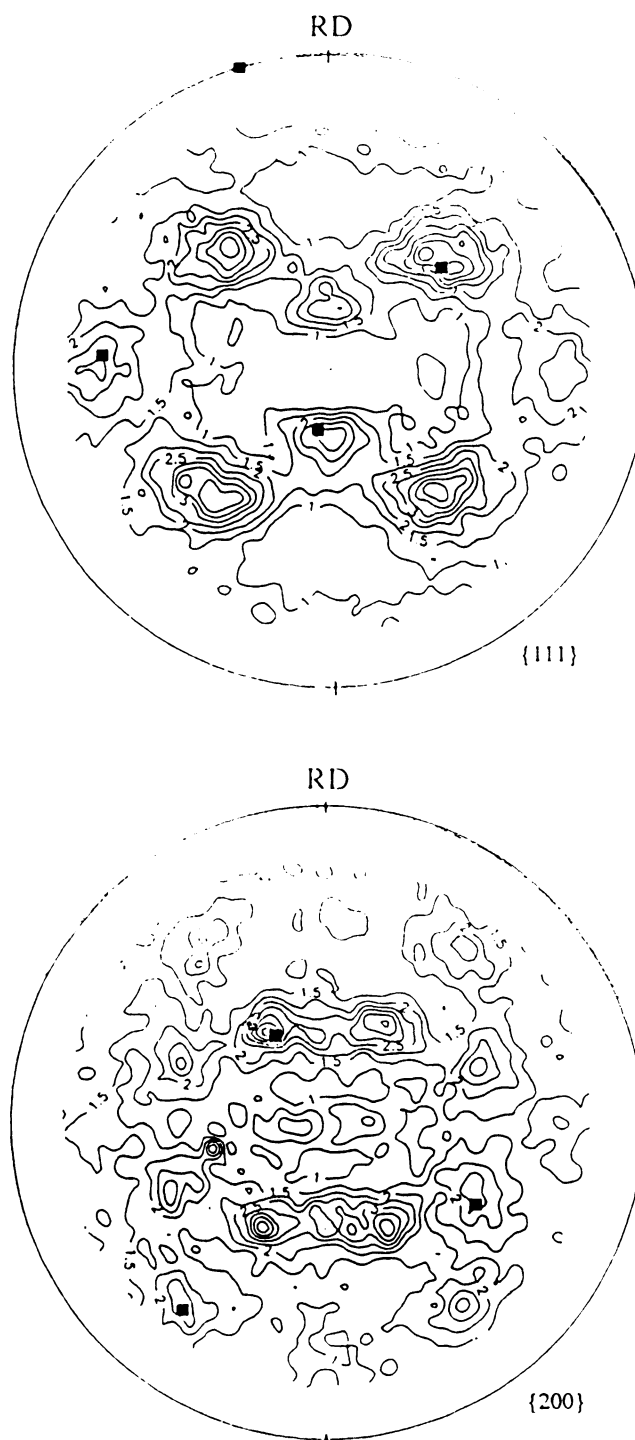


**Figure 4.6.** Recrystallization texture of a aged Cu5%Ag  
after annealing at 550° C.





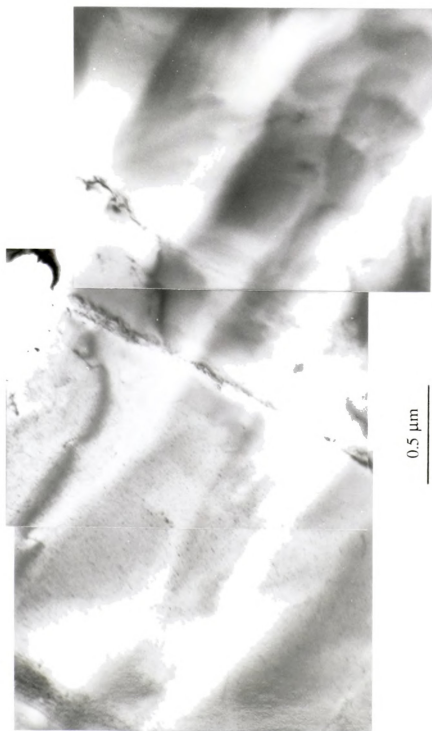


Figure 4.7. TEM micrograph of a single phase Cu5%Ag before rolling.

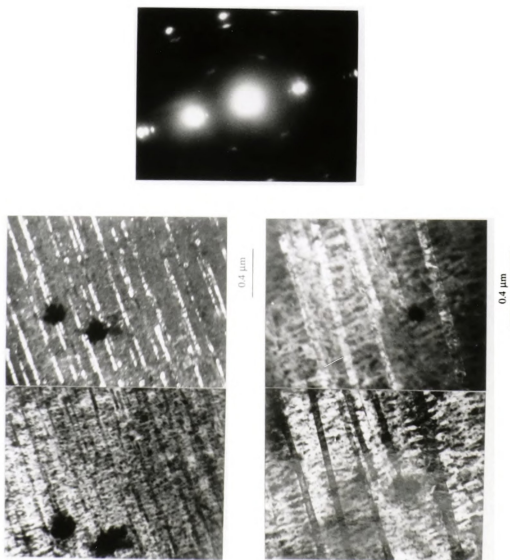
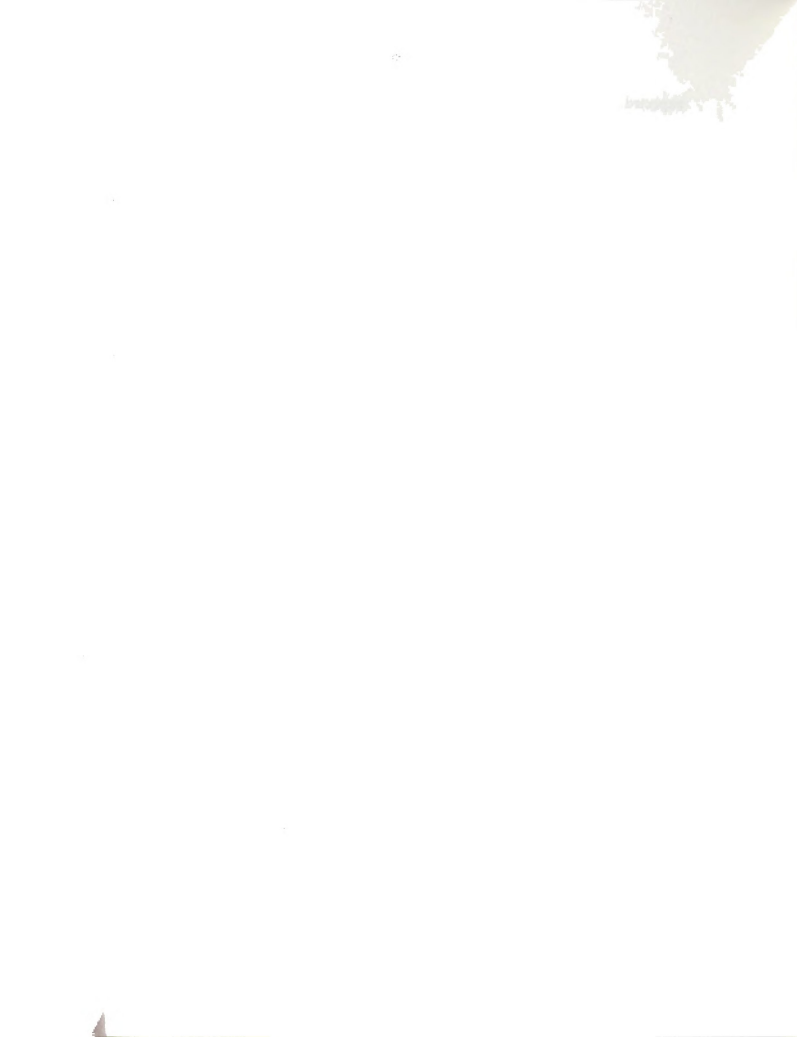


Figure 4.8. Microstructure of a aged two phase Cu5%Ag.

expected a second phase is already distributed throughout the primary phase. During annealing the supersaturated solid solution becomes unstable and decomposes into two phases. The alternate lamellar arrangement of matrix and precipitated phase is the typical microstructure after discontinuous precipitation. The comparison of the micrograph and the corresponding diffraction pattern gives evidence of an alignment of the precipitates parallel to a  $\langle 110 \rangle$  crystallographic direction. The pattern comprises both the matrix and precipitate diffraction, each diffraction spot cluster consisting of matrix and precipitate components and the associated double diffraction spots ( $a_{Cu}/a_{Ag} = 3.61/4.09$ ). A dark field image with the indicated diffraction spot reveals that only rod shaped precipitates which are aligned along a  $\langle 110 \rangle$  direction belong to the corresponding orientation. Thus weak extra spots near the vicinity of the transmitted spot whose zone axis is close to  $\langle 111 \rangle$  may arise from smaller globular precipitates or rods extending in a mainly perpendicular direction of the image plane.

Optical micrographs of the deformation microstructure of the solution treated alloy are shown in Fig. 4-9(a). Longitudinal sections of the specimen rolled to 90% reduction showed microstructures similar to that found in medium stacking fault energy material. The microstructure consisted of deformation bands and Cu type shear bands. Cu type shear bands are known to make an angle of  $35^\circ$  with respect to the rolling plane [8]. Deformation bands are aligned such that their boundary is parallel to the rolling plane. Electron micrographs of the same specimen rendered more detailed features than the optical micrographs. Fig. 4-10(a) shows the Cu-type shear band lying at about  $35^\circ$  to the rolling direction. Higher magnification (Fig. 4-10(b)) shows clusters of microbands aligned parallel to the rolling direction. The micrograph of the highest magnification clearly reveals a long band like feature of  $\sim 0.1\mu\text{m}$  thickness. Selected area diffraction pattern from this regions near  $[111]$  shows elongated diffraction spots. This is due to the fact that a distorted grain has split into regions of



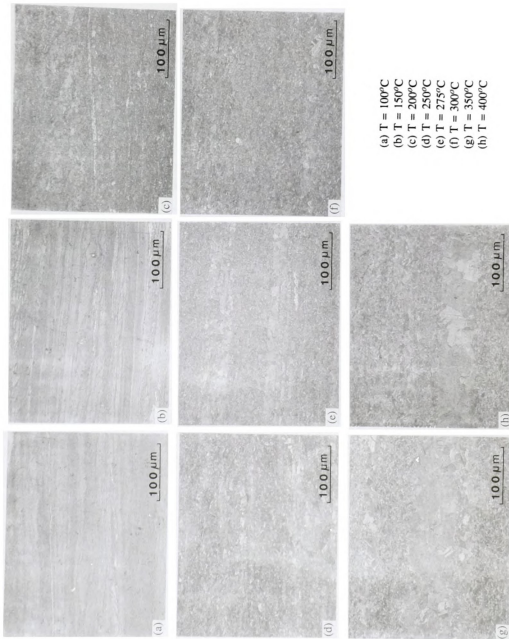


Figure 4.9. Microstructure of 90% cold rolled single phase Cu5%Ag after annealing at various temperature.

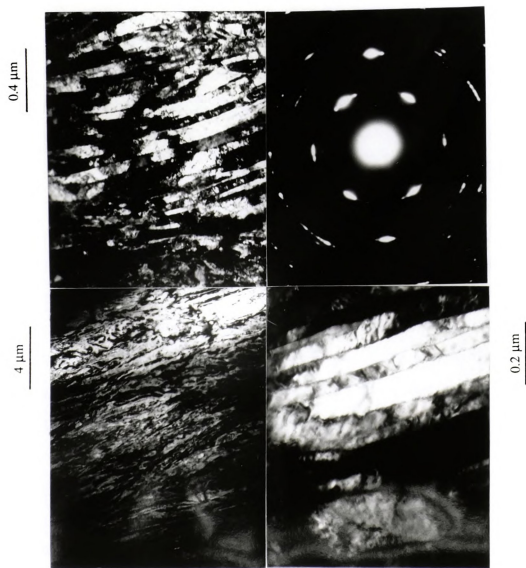


Figure 4.10. TEM micrographs and diffraction pattern of a single phase Cu5%Ag after 90% rolling.

slightly different orientations. In Fig. 4-11 a section in the plane RD-ND is shown in which cube oriented region exist. The SAD pattern taken from upper region of the deformation band shows that this area belongs to a cube orientation. The other SAD pattern taken from the lower region shows that this region is rotated about  $[100]$  (i.e. TD)  $\sim 20^\circ$ . Thus the boundary dividing these two regions is a high angle grain boundary instead of the transition band boundary observed in Fig. 4-10.

The specimen aged at  $600^\circ\text{C}$  before rolling shows features similar to that of the solution treated specimen. Fig. 4-12(a) shows the optical microstructures after 90% reduction. A band like structure is shown parallel to the rolling direction as observed in the single phase alloy. But in the two phase alloy shear bands lying at about  $35^\circ$  to the rolling direction look more like brass type shear bands since the bands are intersecting each other and bounding the rhombic area of the twinned structure. Even though the microstructure in Fig. 4-12(c) was annealed during isochronal tests the area of much broader shear bands is shown clearly to compare with copper type shear bands which are limited to small regions. However it was confirmed that shear bands do not affect the formation of copper type rolling textures despite the large orientation difference between shear bands and the surrounding area [30]. An electron micrograph of the same sample is shown in Fig. 4-13. The microstructure of the aged alloy is quite different from the corresponding microstructure of the supersaturated solid solution. Here the precipitates which were rod shaped before rolling are now elongated along the rolling direction. These elongated precipitates exactly look like fibers of high aspect ratio in a composite material. The comparison of micrograph and diffraction patterns reveals that these fiber like precipitates are aligned along a  $\langle 110 \rangle$  crystallographic direction. In addition to fibrous precipitates much smaller globular precipitates exist also, which which are likely to cause extra weak spots around the transmitted spot whose zone axis is  $[111]$ .





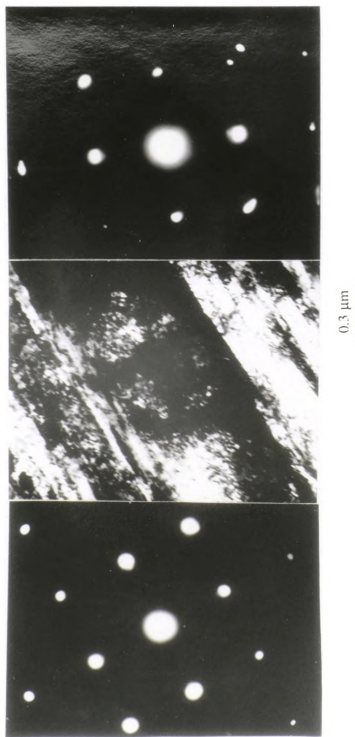


Figure 4.11. TEM micrograph and diffraction patterns of a single phase Cu5%Ag showing deformation bands.

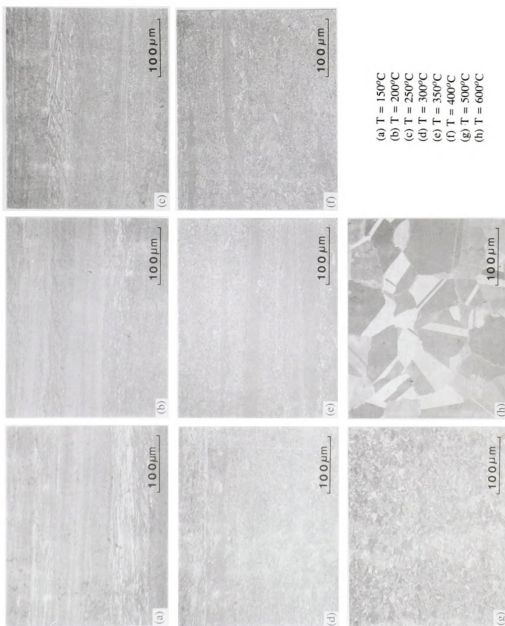


Figure 4.12. Microstructure of 90% cold rolled aged two phase Cu5%Ag after annealing at various temperature.

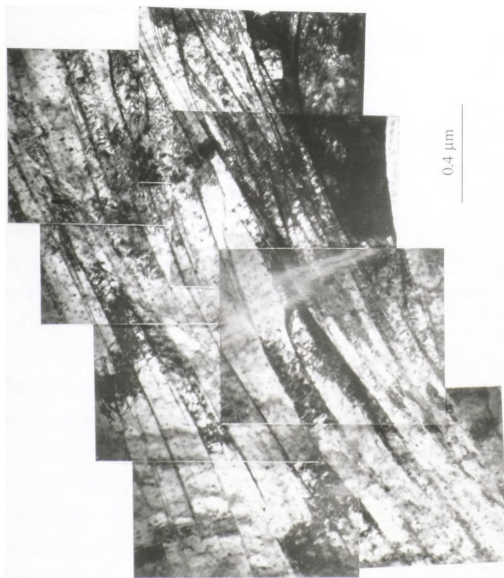
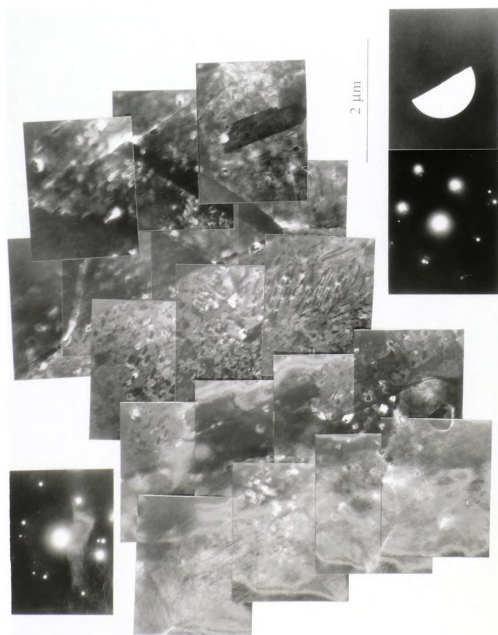


Figure 4.13. TEM micrograph aged two phase Cu5%Ag before rolling.

#### 4.4 Recrystallization Microstructure

Fig. 4-14 shows transmission electron micrograph of a supersaturated alloy rolled to 90% and annealed for 30min. at  $250^{\circ}$ . The specimen is fully recrystallized. Three recrystallized grains which are elongated along the rolling direction (i.e.  $\langle 110 \rangle$ ) can be observed from right to left. The pancake shaped grain structure is retained even after recrystallization. Annealing twins are shown in each pancake shaped grain. The corresponding diffraction pattern (Fig. 4-14(b)) confirms the occurrence of annealing twins. This diffraction pattern also shows that the precipitates are coherent with the matrix since each diffraction spot cluster consists of a matrix and precipitate component and the associated double diffraction spots. Whereas most precipitates have rod shapes, some have sphere shapes of different size. Actually rod shape precipitates are seen as small sphere shape precipitates since they are almost normal to the specimen surface. On the other hand, the formation of large sphere shape precipitates seems to be due to precipitate growth at the expense of smaller precipitates. Fig. 4-15 shows the microstructure of the same sample within a different grain. The overall impression is the same but the concurrent occurrence of recrystallization and discontinuous precipitation is shown more clearly compared with the one shown in Fig. 4-14. In the upper left grain the rod shape precipitates do not extend to the adjacent grain boundary, and rather large globular precipitates dominate in such regions. This may be due to the fact that the area denuded of fibrous precipitates corresponds to the nucleus position with its boundary having moved away during recrystallization or precipitation prior to recrystallization.

The specimen annealed at  $450^{\circ}\text{C}$  shows features similar to the specimen annealed at  $250^{\circ}\text{C}$ . A recrystallized grain several micrometers in diameter is shown in the center. The precipitate morphology is more heterogeneous, comprising longer and also shorter rods and even globular shapes. Note that with increased annealing



1 PHASE  $T = 250^{\circ}\text{C}$

Figure 4.14. TEM micrographs and diffraction pattern of a single phase  $\text{Cu5\%Ag}$  annealed at  $250^{\circ}\text{C}$ .

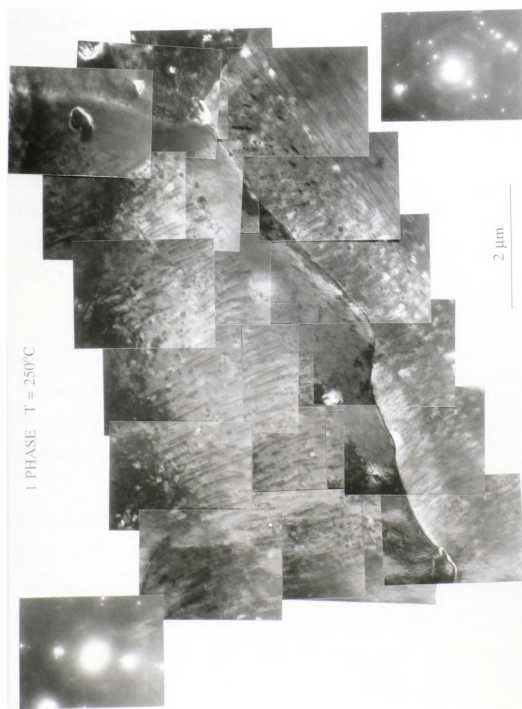


Figure 4.15. TEM micrographs and diffraction pattern of a single phase Cu5%Ag annealed at 250°C.

temperature the grain size is not significantly changed. Fig. 4-16 shows the microstructure of the same specimen inside the grain boundary. Although no matrix grain boundary is apparent in the area under focus the diffraction pattern contains several orientations. In Fig. 4-17(c) a dark field image is obtained at the spot near the (110) spot. Since the size of field limiting aperture is large enough to cover some portion of the 1st ring pattern near the (110) spot the the changed contrast of the precipitates belongs to both coherent and incoherent precipitates. The ring pattern seems to come from randomly oriented small precipitate particles of globular shape. Since the radius of each ring is related to the interplanar spacing of reflecting planes the ring pattern can be indexed using the following equation.

$$R \times d = \lambda \times L \quad (4.1)$$

where R = radius from the diffracted spot to the center

d = interplanar spacing

$\lambda$  = electron wave length

L = camera length

Table 4-1 shows a list of the interplanar spacings of matrix and precipitates in the Cu-5wt%Ag alloy.

The recrystallized microstructure of the aged alloy is quite different from the corresponding microstructure of the supersaturated solid solution alloy. Fig. 4-18 shows a transmission electron micrograph of an aged alloy rolled to 90% and annealed for 30min. at 100° C. A recrystallized grain which was submicron in diameter started to grow in a highly deformed region which had very elongated fibrous precipitates. Concomitant with the recrystallization, globular precipitates 0.1 to 0.3  $\mu\text{m}$  in size were found to form at the recrystallization front and inside the newly recrystallized grain at the expense of the long fiber precipitates in the deformed region. Fig.

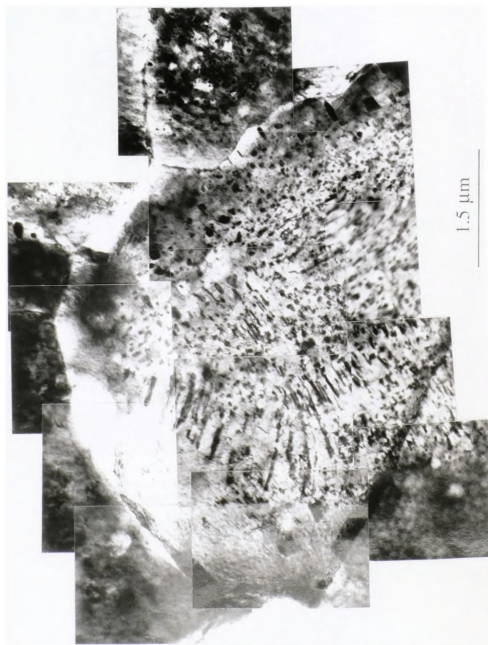
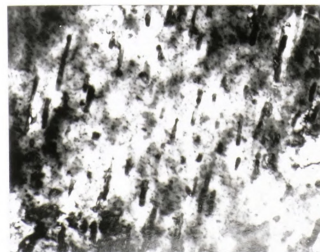
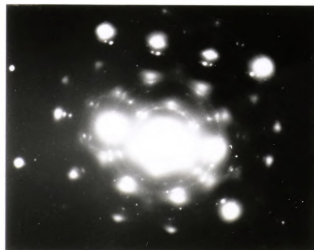
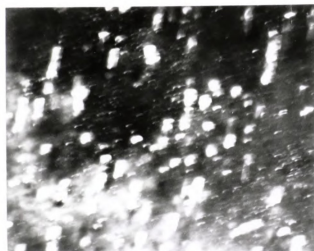


Figure 4.16. TEM micrograph of a single phase alloy after annealing at 450°C.



1 PHASE T = 450°C



0.6  $\mu\text{m}$

Figure 4.17. TEM micrographs and diffraction pattern of a single phase Cu5%Ag annealed at 450°C.

hkl	d (5wt%Ag)		
	solid solution	two phase	
111	2.101	m	2.087
		p	2.359
200	1.819	m	1.808
		p	2.044
220	1.286	m	1.278
		p	1.445
311	1.097	m	1.090
		p	1.231
222	1.050	m	1.044
		p	1.180

**Table 4.1** List of the interplanar spacings of matrix and precipitates

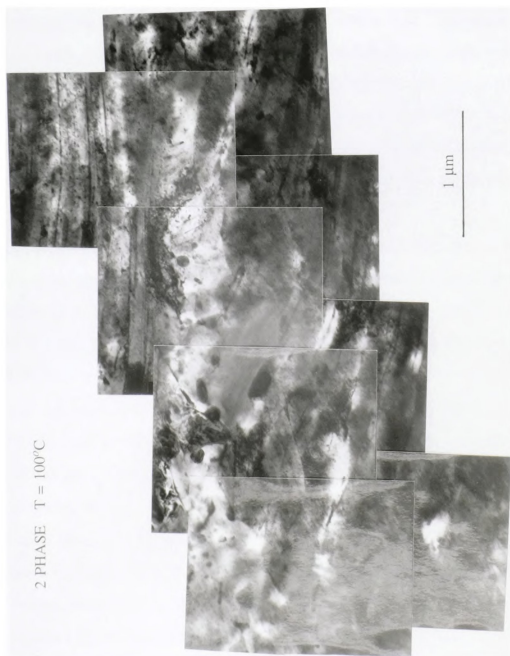


Figure 4.18. TEM micrograph aged two phase Cu5%Ag annealed at  $100^{\circ}\text{C}$ .

4-19 shows the microstructure of the same specimen in a different area. Here again similar features are shown but the size of the recrystallized grain is much larger while the size of the precipitates are almost the same compared with the microstructure shown in Fig. 4-18. A selected area diffraction pattern taken from lower left grain has a cube orientation while the selected area diffraction pattern taken from the deformed region shows an orientation close to  $\{011\}\langle 100 \rangle$ . The comparison of both diffraction patterns reveals an orientation relationship between them which is a  $45^\circ$  rotation around the axis close to the  $\langle 100 \rangle$  direction. However the orientation relationship between upper grain and deformed region is a  $45^\circ$  rotation around the axis close to the  $\langle 110 \rangle$  direction.

The microstructure of an aged alloy sample annealed at  $200^\circ\text{C}$  (Fig. 4-20(b)) shows features similar to annealed at  $100^\circ\text{C}$ . It is clearly shown that fibrous precipitates transform to globular precipitates 0.1 to 0.3  $\mu\text{m}$  in size upon recrystallization of the matrix phase. The increase of the annealing temperature enhances the progress of recrystallization and increases the recrystallized area.

After annealing at  $300^\circ\text{C}$ , a large area was recrystallized which contained large globular precipitates and also fine needle shape precipitates. Fig. 4-21. shows a recrystallized grain several  $\mu\text{m}$  in size which is slightly larger than those annealed at lower temperatures.

Drastic changes in the microstructure of the aged alloy occur after annealing at a higher temperature of  $550^\circ\text{C}$ . Here the morphology of precipitates is totally different from those annealed at a lower temperature. While the large globular shape precipitate and the fine needle shape precipitate do not appear, extremely fine globular precipitates are distributed randomly. As evident from the optical micrograph, the grain boundary can not be found through TEM due to a 50  $\mu\text{m}$  diameter grain size after grain growth. A selected area diffraction pattern from the microstructure in Fig. 4-22(b) shows typical ring pattern. This can only be due the existence of the



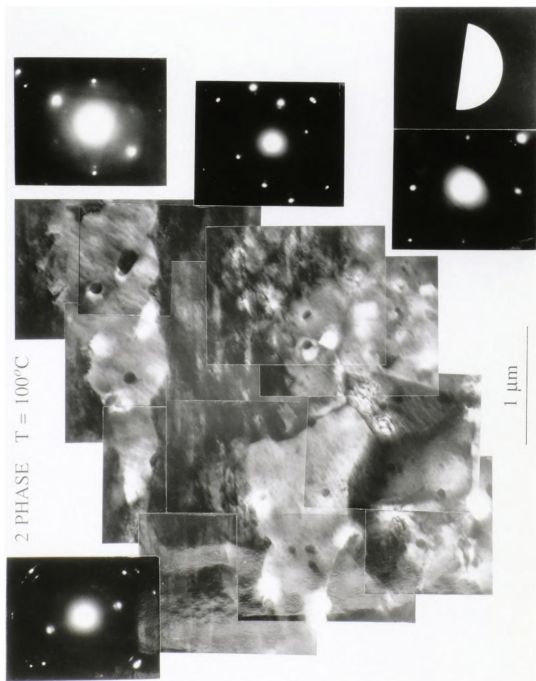


Figure 4.19. TEM micrographs and diffraction pattern of aged two phase Cu5%Ag annealed at 100°C.

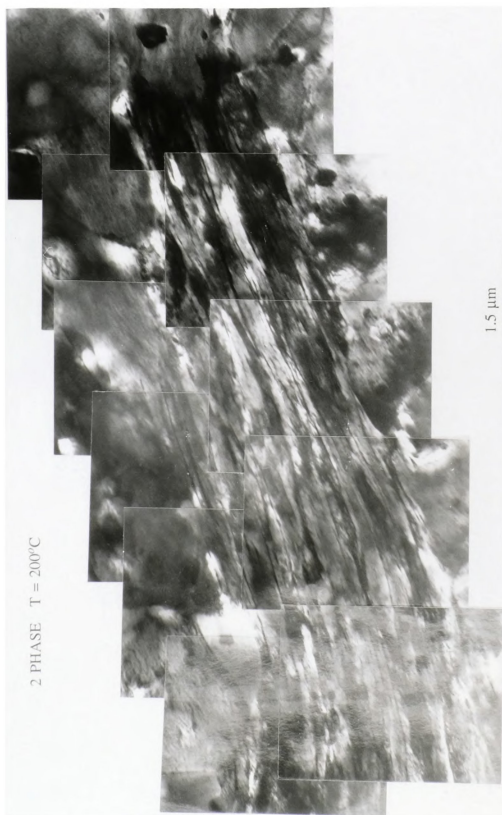


Figure 4.20. TEM micrograph aged two phase Cu<sub>45</sub>%Ag annealed at 200°C.

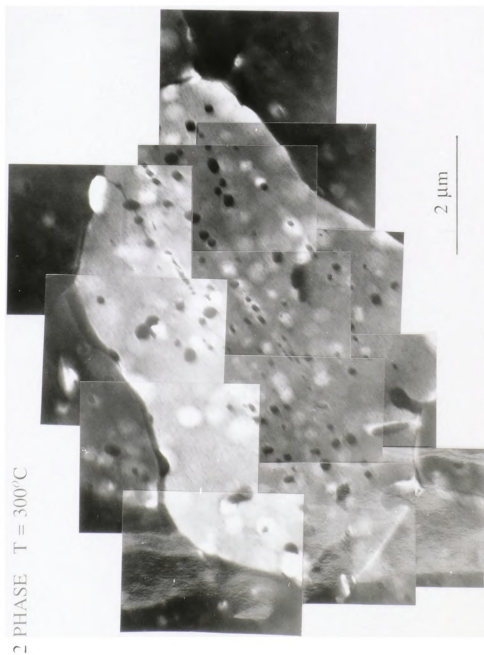


Figure 4.21. TEM micrograph aged two phase Cu5%Ag annealed at 300°C.





2 PHASE  $T = 550^{\circ}\text{C}$

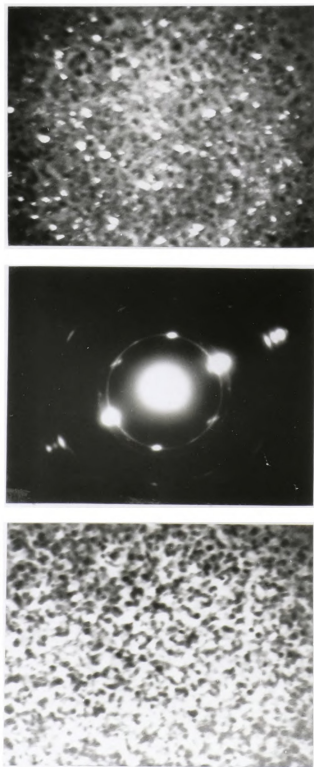


Figure 4.22. TEM micrographs and diffraction pattern of aged two phase Cu5%Ag annealed at  $550^{\circ}\text{C}$ .



randomly oriented small precipitates. However some of them are still coherent with the matrix phase since the intensity near the (110) diffraction spot is obviously much stronger than the average intensity along the ring. In Fig. 4-22(c) a dark field image is obtained from the spot near (222). The precipitates with the changed contrast are coherent with the matrix phase.

#### 4.5 Hardness

The recrystallization kinetics of the rolled samples in both single and two phase become obvious from annealing and hardness isochronal tests. A major drop in hardness occurs between 200°C and 300°C for the single phase specimen and a similar drop occurs between 300°C and 400°C. From these data it can be concluded that primary recrystallization was completed at 250°C for the single phase alloy and 350°C for the two phase alloy. This was also confirmed by optical microscopy. Note that a small but obvious hardness increase is shown at 100°C for the single phase alloy. The results of the isochronal test (Fig. 4-23) between 100°C and 300°C at intervals of 20°C clearly shows the same phenomena. A similar hardness increase has been found in other alloys such as the Cu-Zn, Cu-Al, and Cu-Si alloys by Mohan et al. [48]. Two possible mechanisms of this increase have been proposed. Clarebrough et al. [49] proposed that the short range order during low temperature annealing is the cause for this strength increase. On the other hand, Suzuki [50] suggested that the strengthening is due to the segregation at stacking faults, which becomes a barrier to dislocation motion.

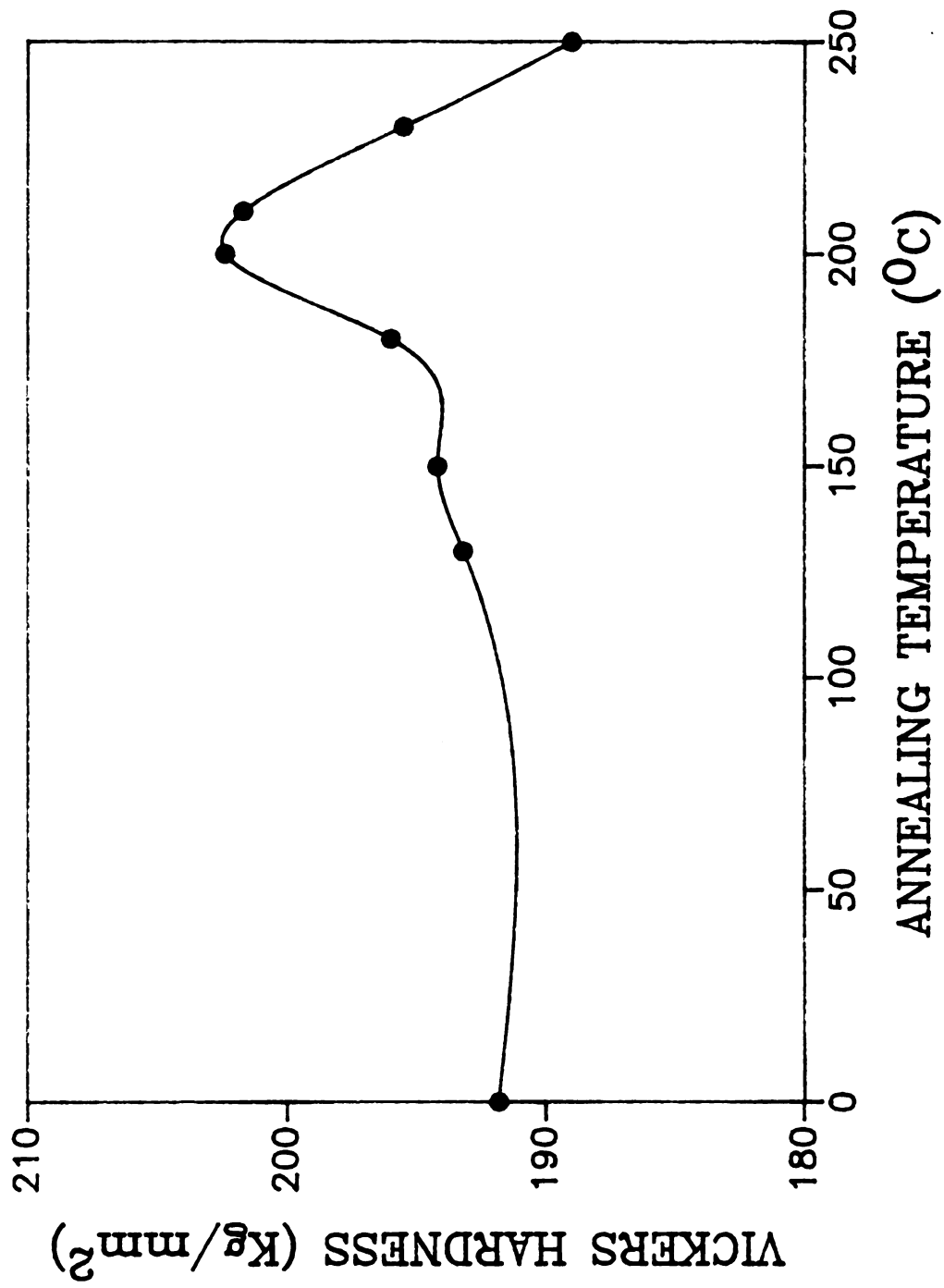


Figure 4.23. Vickers hardness as function of temperature for 30 min. isochronal annealing for 90% rolled Cu5%Ag.



## 4.6 Stored Energy Measurements

The results for a solid solution alloy rolled to 95% reduction are shown in Fig. 4-24(a). The slope of the baseline is due to the different heat capacities of the sample and the reference. The stored energy release occurs at about 300° C. Fig. 4-24(b) shows more precisely the interval of stored energy release. Its occurrence at 300° C is quite in agreement with the results of hardness measurements and metallography. The value of stored energy, which by definition is identical with the driving force for primary recrystallization, is 2.258J/g. This value is relatively large compared with other materials [57-59]. But, in the present case, a chemical driving force released during the combined recrystallization and precipitation and the elastic energy of the removed dislocations contribute to the total driving force of the discontinuous recrystallization.

## 4.7 Tensile Test

Mechanical properties of both single phase and two phase alloys in their longitudinal directions were measured at room temperature in the rolled and aged state. The plots of engineering stress vs. engineering strain are shown in Fig. 4-25,26,27. A summary of mechanical properties is presented in Table 4-2. From this table, it is evident that rolled samples have much higher strength but lower ductility, and the rolled two phase alloy shows the highest yield strength(i.e. 260MP) but the lowest ductility. The yield strength of the rolled two phase alloy is higher than that of the solid solution alloy. As already shown in TEM micrographs, the rolled two phase alloy has elongated fibrous precipitates which are aligned along the rolling direction as in a fiber reinforced composite. The increase in strength can be associated with this reinforcement. The mechanical strength of the fine grained metal is much higher

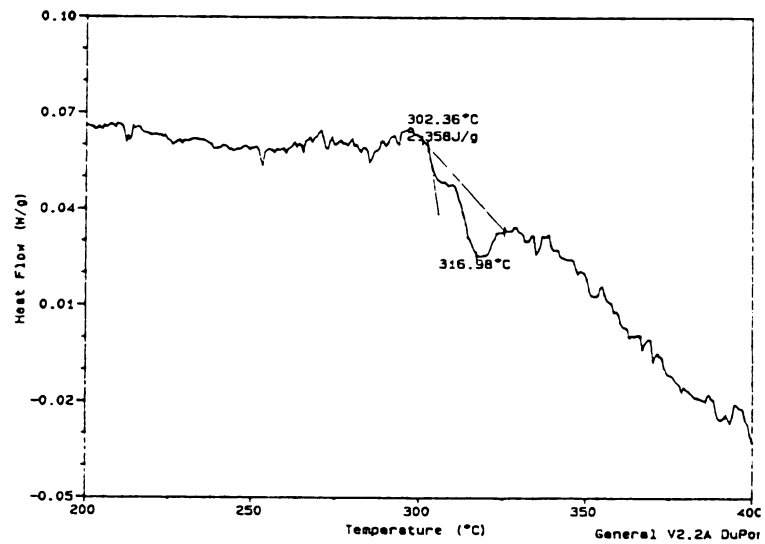
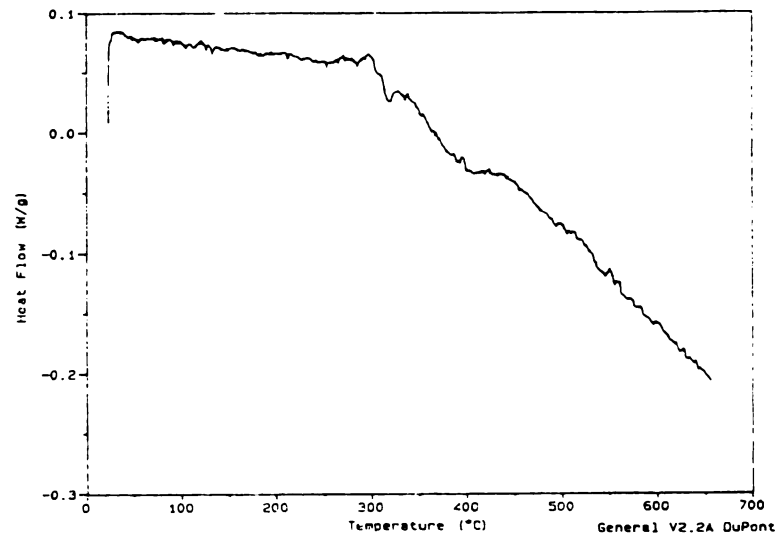
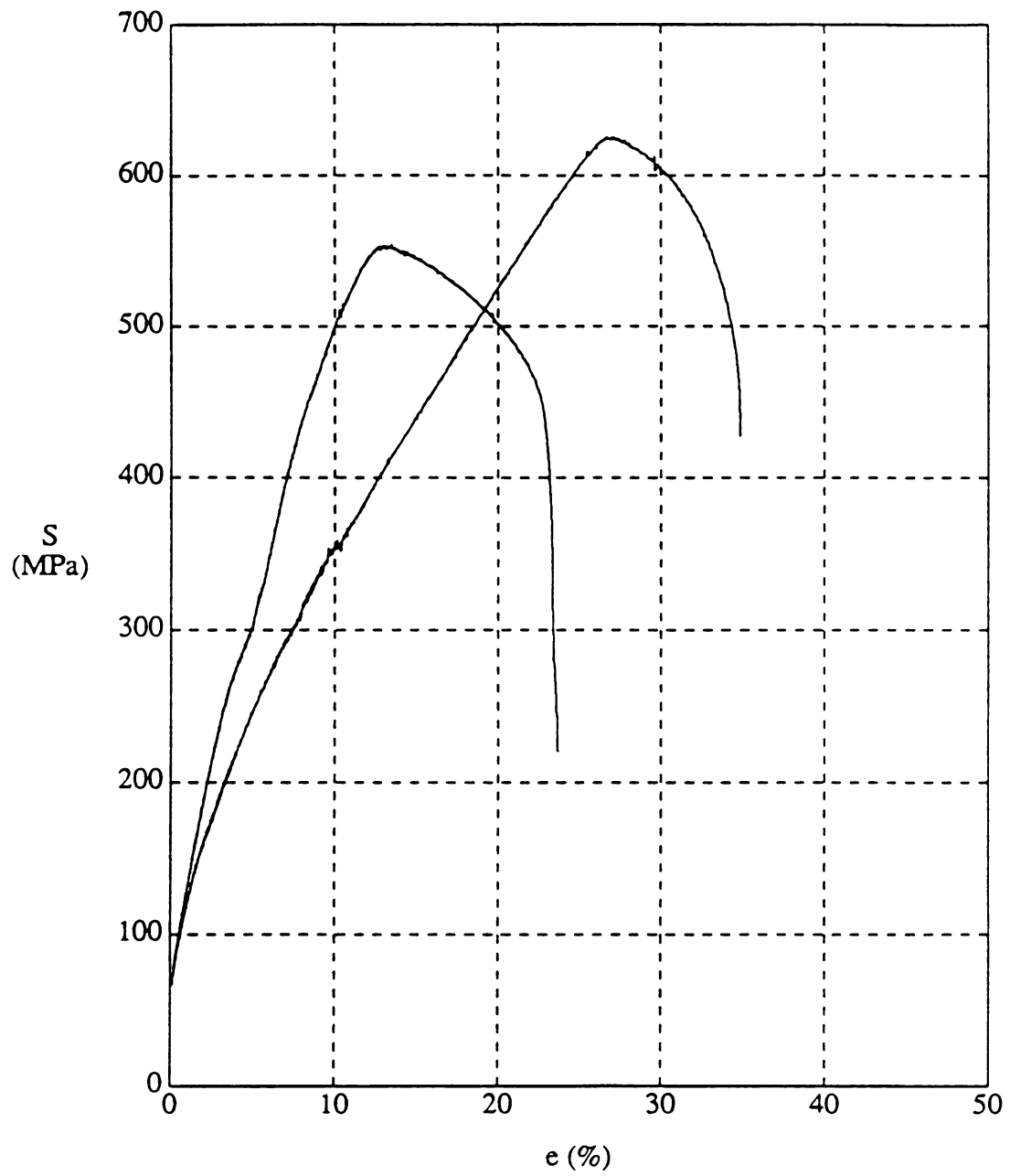


Figure 4.24. Stored energy release of a solid solution alloy rolled to 95% reduction.





**Figure 4.25.** The engineering stress-strain curve after rolling: (a) solid solution alloy  
(b) aged two phase alloy.



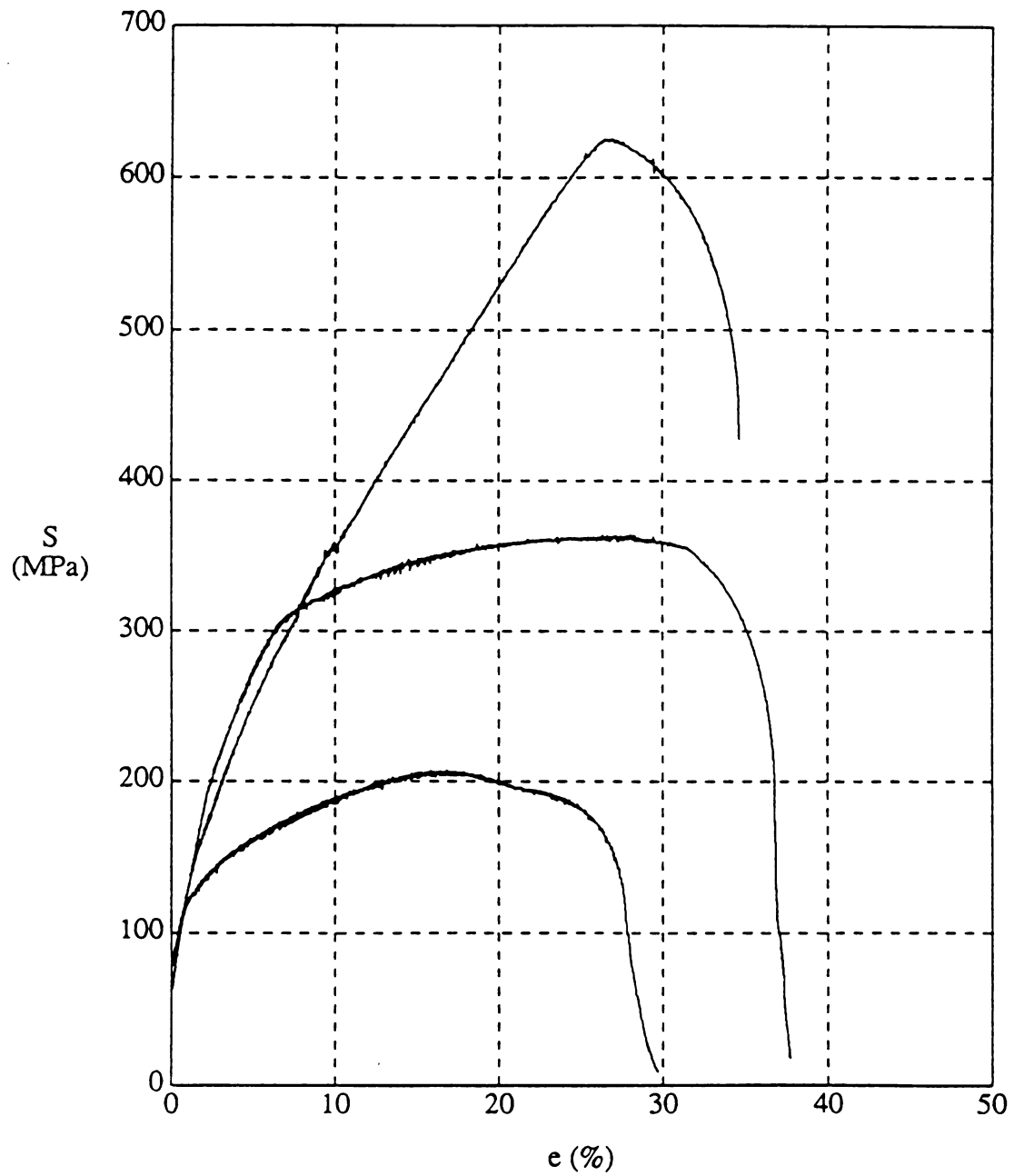


Figure 4.26. The engineering stress-strain curve of a solid solution alloy: (a) after rolling  
(b) after annealing at 250° C.  
(c) after annealing at 450° C.

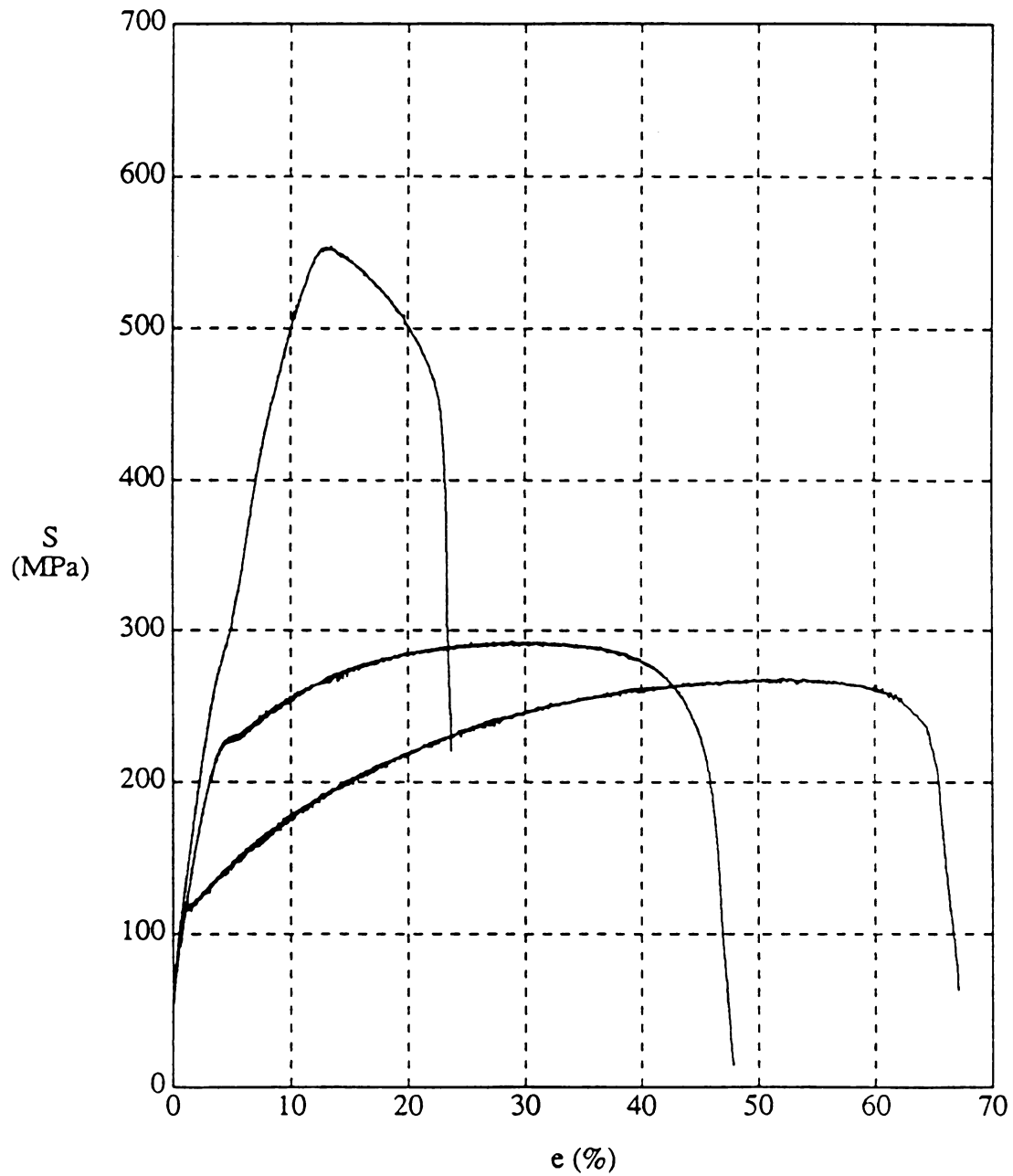


Figure 4.27. The engineering stress-strain curve of a two phase alloy: (a) after rolling  
(b) after annealing at 350° C.  
(c) after annealing at 550° C.

Specimen		$S_y$ (Mpa)	UTS (Mpa)	$e_f$ (in %)
Solid solution 1 phase	rolled	152	626	35.7
	250 °C	200	358	37.8
	450 °C	105	207	29.7
Aged 2 phase 2 phase	rolled	260	552	23.6
	350 °C	190	291	47.8
	550 °C	118	267	67.4

Table 4.2 Yield Limit Response Data



than that of the coarse grained metal, since the dislocation structure of the deformed structure is destroyed by the recrystallization. Thus, the degradation in tensile strength by annealing can be attributed to a recrystallization process.

The improved yield strength of the single phase alloy after annealing at 250° C corresponds to the results of microhardness measurements. Again this improvement may be due to short range order or the Suzuki effect.

## CHAPTER 5

### DISCUSSION

#### 5.1 Precipitation and Recrystallization

Although not observable by optical microscopy, fine continuous precipitates have been observed through TEM after various stages of annealing from both the supersaturated solid solution and the aged two phase material. While the precipitates have small spherical shapes in the aged two phase material and the two phase material annealed at 550°C, the shape is fine needle-like in all other cases. This observed difference may be due to the undeformed microstructure or enlargement of the needle like precipitate during relatively high temperature annealing. In accordance with early findings, the fine continuous precipitates have Widmanstatten morphology and are aligned along  $\langle 110 \rangle$  as shown in Fig. 4-14 and Fig. 4-17. From the SAD pattern it is apparent that these precipitates are coherent with the matrix phase. These fine precipitates are distributed throughout the volume, seemingly neither to be dissolved nor to be passed through by the motion of the moving grain boundaries.

The alternative case is observed in discontinuous precipitation and continuous precipitation of relatively large particles compared with the much smaller continuous precipitate mentioned above. In the aged two phase alloy the elongated fibrous precipitate is dissolved completely by the migrating grain boundary, and large globular particles precipitate at the grain boundary and also inside the newly formed grain. In this case coherent precipitates reprecipitate coherently with the growing grain, as was frequently observed in a variety of alloy systems [41,42,43]. Similar features can be observed in the supersaturated solid solution alloys. Relatively large globular shape





particles form in the precipitate free zone ( only for large scale precipitates ) behind the grain boundary. This area seems to be the portion where the grain boundary moved away during grain growth immediately following the combined discontinuous reactions.

As already mentioned fine continuous precipitates have been observed frequently after annealing of the deformed alloys. It is hard to tell whether the fine scale precipitates are the result of continuous precipitation or spinodal decomposition on the basis of electron microscopy [51]. However a miscibility gap has been constructed on the equilibrium phase diagram by Boswell et al. [52] using an equation of Cook et al. [53]. The occurrence of spinodally decomposed structures is easier in the deformed alloy compared with the undeformed alloy [54]. It was also shown that the elastic strain energy caused from the coherency strain lowers the temperature of spinodal decomposition [55]. Then, in the present case, the occurring temperature of spinodal decomposition seems to be lowered additionally.

Drastic changes in the morphology of the precipitates occurs after annealing of the two phase alloy at 550°C. Small globular precipitates about 20nm in diameter are dispersed within the matrix. The two phases seem to form a coherent interface to attain the lowest free energy since the Ag rich precipitate has the same crystal structure and a similar lattice parameter. Actually the atomic size difference is large (11.6%) compared with a system such as Al-Ag (0.97%), which forms fully a coherent precipitate. The matrix and precipitate must be strained to maintain a coherent interface. These precipitates seem to have been formed after the completion of recrystallization. It seems that long fiber like precipitates have been dissolved completely by the motion of the recrystallization front. Small globular precipitates have also been formed continuously behind the moving grain boundary. Thus precipitate are formed in the strain free region different from other cases such as discontinuous or localized precipitation. This could be the reason for the formation of different

morphology in both size and shape.

In the supersaturated solid solution alloy recrystallization and discontinuous precipitation occurred simultaneously after annealing at 250°C and 450°C. The difference in annealing temperature seems not to affect the sequence of recrystallization and precipitation. But, as seen in the optical micrographs, grain growth occurred after the completion of combined discontinuous reactions in the specimen annealed at 450°C. After recrystallization, grains grow further during continued annealing. During this grain growth it seems that moving grain boundaries bypass the coherent precipitates, and then these precipitates become incoherent with the matrix phase. The occurrence of an apparent ring pattern in single phase alloys annealed at 450°C would support this interpretation.

## 5.2 Texture

The rolling textures are very much as expected. While pure copper develops a Cu type rolling texture, its concentrated alloys tend to form a brass type texture [9-13]. With increasing solute content the Cu type rolling texture changes to a transition type texture and finally to the brass type rolling texture. According to the pole figures both the single and two phase alloy exhibit a transition type texture. It seems obvious that 5% Ag in Cu content can decrease the stacking fault energy low enough to cause texture transition. The transition of the rolling texture observed for the present alloy is similar to that observed in the Cu-Zn [11], Cu-P [12], and Cu-Ge [13]. Only the amount of alloy content to cause the texture transition is different in such a way that 5% Ag corresponds to 6% Zn, 1% P, and 2% Ge respectively. Thus, only one parameter, the stacking fault energy, apparently causes the rolling texture transition.

According to present results there is no evidence to distinguish the rolling texture of the solid solution alloy from that of the two phase alloy. Here the aging treatment prior to rolling to produce the second phase has little effect on the subsequent deformation behavior. Even though a second phase is distributed throughout the matrix phase as the long fibrous shape already shown in TEM micrographs, the deformation texture is almost the same as that of the single phase alloy. From this result it can be concluded that the motion of dislocation or mechanical twinning was not notably affected by the presence of a second phase. This may be attributed to the fact that the second phase (i.e. silver rich precipitate) has deformation characteristics similar to copper alloys.

After annealing one finds different textures for the supersaturated solid solution alloy and the aged two phase alloy. In the first case the resulting texture varies with the annealing temperature. While the cube orientation can be found at both annealing temperatures, other details differ. From the pole figure it can be noted that the intensity of the cube component gets stronger with the increase in the annealing temperature. This is probably due to grain growth, since the annealing texture continues to develop after completion of recrystallization. Although there is a minor difference in the texture components the annealing texture of the solid solution alloy develops by combined discontinuous reactions as evident from the TEM micrographs. In the second case ( i.e. aged two phase alloy ), the recrystallization textures annealing at for both  $350^{\circ}\text{C}$  and  $550^{\circ}\text{C}$  is a mixed texture comprising retained rolling and cube texture. This implies that continuous recrystallization ( recrystallization in situ ) is the major mechanism which leads to the partial retention of the rolling texture, while the cube component belongs to the portion which has been recrystallized discontinuously. The occurrence of a cube component seems to be due to rapid growth of cube oriented nuclei since they undergo recovery and recrystallization much faster than the nuclei of other orientations during the early stage of recrystallization [17,18].

The observations in the supersaturated solid solution are far more complicated owing to the concurrent occurrence of precipitation and recrystallization. Hornbogen and Kreye [2] (referred to as HK in the following) investigated a variety of commercial alloys Al-Cu, Ni-Al, Ni-Cr-Al, Cu-Co, Ni-Be and found that a discontinuous recrystallization always leads to a random texture even from a pronounced deformation texture, and they attribute their result to a loss of growth selection owing to impurity drag because of segregation of the solute to the grain boundaries. The present results cannot confirm the observation of HK.

The cube orientation is known as an orientation to develop very early during recrystallization [19]. According to current understanding of cube texture formation [18,20,21], it first nucleates in the Cu component of the rolling texture and then favorably grows into the S component. This is consistent with the present results, since both Cu and S orientation are identified in the rolling texture. In conclusion, the recrystallization textures can be basically accounted for by the known recrystallization mechanisms for texture formation in solid solutions. This implies also that the observed crystallographic growth of the discontinuous precipitates, which actually provides the major driving force for grain boundary migration during recrystallization does not noticeably affect the growth of the recrystallized grains.

It is not quite clear what causes the difference between the current investigation and the results of HK on other systems. HK surmise that the texture randomization is due to a loss of growth anisotropy owing to segregation. This may indeed be correct for the systems that they studied. However, it certainly cannot be generalized, otherwise recrystallization texture formation in single phase alloys could be ruled out in general, quite in contrast to common observations, e.g. in the well studied system Cu-Zn. Without any doubt the extent of segregation and consequently its effect on grain boundary mobility depends strongly on the alloying element. For example it is well known that Cu or Mg additions to Al effectively reduce the recrystallization

kinetics, while alloying of Al with Ag hardly has any effect on the recrystallization of Al. Therefore, each alloy system has to be considered differently. From our results we have to conclude that also alloying of Cu with Ag does not substantially change the recrystallization mechanisms operating in pure Cu. In fact, the rolling and recrystallization textures as established in this investigation are qualitatively very similar to results on Cu6%Zn [63], essentially consisting of the same components, although different in strength.

In the rolled single phase alloy the presence of a cube oriented region was identified in the transition band area by means of SAD patterns in the electron microscope. The existence of a cube orientation in the deformed structure is important to the argument about whether the cube texture is developed by oriented growth or oriented nucleation. The cube oriented region located in the thin band region elongated along the rolling direction and the large angle grain boundary separates the cube oriented band from its neighbor deformation band. Dillamore et al. [16] proposed a model for the formation of the cube orientation in f.c.c. materials, saying that the cube orientation can be formed in the transition band region during deformation. Their model predicts that certain orientations rotate around the normal direction to approach the cube orientation and then rotate further around the rolling direction to form the cube orientation. In agreement with other authors [16,18] the cube orientation can be identified in the ND-RD plane. From the corresponding SAD pattern it is evident that the cube oriented grain is separated from its neighbor by a large angle grain boundary. It is worthwhile to note that the cube oriented band is rotated around the rolling direction with respect to its neighbor as predicted by Dillamore et al. [16]. During annealing this large angle grain boundary can migrate rapidly due to its high mobility.

## CHAPTER 6

### CONCLUSIONS

The main results are summarized as follows:

- 1) Discontinuous precipitates present prior to rolling, which are coherent with the matrix phase, tend to deform with the matrix becoming fibrous shaped.
- 2) Annealing of the deformed supersaturated solid solution alloys at 250°C and 450°C leads to the formation of a fine continuous matrix precipitation followed by a combined discontinuous reaction of recrystallization and precipitation. The migrating grain boundary bypasses fine continuous precipitates but leaves fibrous precipitates at the grain boundary and also inside the newly formed grain. The difference in annealing temperature seems not to affect the sequence of recrystallization and precipitation. But grain growth occurs after the completion of combined discontinuous reactions in the specimen annealed at 450°C. During this grain growth it seems that moving grain boundaries bypass the coherent precipitates and then these precipitates become incoherent with the matrix phase.
- 3) In the two phase alloy the elongated fibrous precipitates are dissolved completely by the migrating grain boundary and large globular particles precipitate coherently behind the moving grain boundary.
- 4) Drastic changes occurs in the morphology of the precipitates during annealing of the two phase alloy at 550°C. While the large globular shape precipitate disappear, small globular precipitates about 20nm in diameter are dispersed within the matrix. These precipitates seem to form after the completion of recrystallization and grain growth.

- 5) The deformed single and two phase alloys exhibit a transition type rolling texture comprising an S orientation  $\{123\}\langle 634 \rangle$ , brass orientation  $\{011\}\langle 211 \rangle$  and Goss orientation  $\{011\}\langle 100 \rangle$ . The aging treatment prior to rolling has little effect on the subsequent deformation texture.
- 6) The recrystallization textures of the supersaturated solid solution alloy annealed at  $250^{\circ}\text{C}$  and  $450^{\circ}\text{C}$  are essentially of transition type texture with the cube orientation  $\{001\}\langle 100 \rangle$  as a major component.
- 7) The recrystallization textures of the two phase alloy for both annealing at  $350^{\circ}\text{C}$  and  $550^{\circ}\text{C}$  are mixed textures consisting of partially retained rolling and cube texture. The cube component is getting stronger due to grain growth as the annealing temperature increases.
- 8) Texture randomization is not observed after discontinuous recrystallization. The crystallographic growth of the recrystallized grains was not influenced noticeably by the concurrent discontinuous precipitation which actually provides the major driving force for grain boundary migration during recrystallization.
- 9) In accordance with the findings of other authors in copper [16,18], the presence of a cube oriented region is identified in the transition band area in the rolled single phase alloy.



## LIST OF REFERENCES

- [1] P. Cotterill and P.R. Mould: *Recrystallization and Grain Growth in Metals*, John Wiley, New York, (1976)
- [2] E. Hornbogen and H. Kreye: in *Texturen in Forschung und Praxis*, ed. J. Grewen and G. Wassermann, Springer Verlag, Berlin, (1969) 274
- [3] E. Hornbogen and U. Köster: in *Recrystallization of Metallic Materials*, ed. F. Haessner, Dr. Riederer Verlag, Stuttgart (1978) 159
- [4] N. Hansen: *Mem. Sci. Rev. Met.* 72 (1975) 189
- [5] E. Hornbogen: *Z. Metallk.* 69 (1978) 735
- [6] S. Saji and E. Hornbogen: *Z. Metallk.* 69 (1978) 741
- [7] C. Zener and C.S. Smith: *Trans. AIME* 175 (1949) 15
- [8] E. Hornbogen: *Prakt. Metallographie* 9 (1970) 349
- [9] U. Schmidt and K. Lücke: *Texture* 3 (1979) 85
- [10] P.A. Beck: *Advances in Physics* 3 (1954) 245
- [11] J. Hirsch and K. Lücke: *Acta Met.* 36 (1988) 2863
- [12] U. Schmidt, K. Lücke and J. Pospieche: *Int. Conf. on Textures*, Cambridge, (1975) 154
- [13] H. Eichelkraut, J. Hirsch and K. Lücke: *Z. Metallk.* 75 (1984) 113
- [14] R. Alam, H.D. Mengelberg and K. Lücke: *Z. Metallk.* 58 (1967) 867
- [15] G. Wassermann: *Z. Metallk.* 54 (1963) 61
- [16] I.L. Dillamore and H. Katoh: *Met. Sci.* 8 (1974) 73
- [17] T. Noda and J. Huber: *Z. Metallk.* 69 (1978) 570

- [18] A.A. Ridha and W.B. Hutchinson: *Acta Met.* 30 (1982) 1929
- [19] J.W.H.G. Slakhorst: *Acta Met.* 23 (1975) 301
- [20] J. Hirsch and K. Lücke: in *Annealing Processes - Recovery, Recrystallization and Grain Growth*, ed. N. Hansen et al., Riso National Laboratory, Roskilde, Denmark (1986) 361
- [21] J. Hirsch, E. Nes and K. Lücke: *Acta Metall.* 35 (1987) 427
- [22] C. Zener and C.S. Smith: *Trans. AIME* 175 (1949) 15
- [23] B. Liebmann, K. Lücke and G. Masing: *Z. Metallk.* 47 (1956) 57
- [24] G. Ibe, W. Dietz, A.C. Fraker and K. Lücke: *Z. Metallk.* 61 (1970) 498
- [25] P. Stuijte and G. Gottstein: in *Proc. 5th Int. Conf. on Textures of Materials*, ed. G. Gottstein and K. Lücke, (1978) 511
- [26] W.G. Burgers, Y.H. Lin and T.J. Tiedema in *The influence of crystal orientation on polygonisation of aluminum single crystals*, *Proc. Nederlandse Akadamie van Wetenschappen.* 54 (1951) 459
- [27] S.P. Bellier and D. Doherty: *Acta Met.* 25 (1977) 521
- [28] H. Hu: in *Recovery and recrystallization of Metals*, ed. L. Himmel, Interscience Publ., New York (1964) 311
- [29] M. Hatherly: in *Proc. 5th Int. Conf. on Textures of Materials*, ed. G. Gottstein and K. Lücke, (1978) 81
- [30] J. Grewen, T. Noda and D. Sauer: *Z. Metallk.* 67 (1977) 260
- [31] A. Kelly and R.B. Nicholson: in *Progress in Materials Science*, ed. B.Chalmrs, Pergamon Press, New York 10 (1963) 149
- [32] F.J. Humphry and J.W. Martin: *Phil Mag.* 17 (1968) 146
- [33] K.H. Virnich, G.Kohlhoff, K. Lucke and J. Pospiech: in *Proc. 5th Int. Conf. on Textures of Materials*, ed. G. Gottstein and K. Lücke, (1978) 475

- [34] J.W. Christian: in *The theory of transformations in metals and alloys*, (1965) Oxford, Pergamon.
- [35] K.C. Russel: in *Phase transformations*, New York, ASM, Chapman and Hall, (1970) 219
- [36] J.W. Martin and R.D. Doherty: in *The stability of microstructure in metallic systems*, Cambridge, Cambridge University Press, (1976) 10, 163, 182
- [37] R.D. Doherty: in *Phase boundaries*, ed. D. Smith and G.A. Chadwick, London, Academic Press
- [38] J.W. Cahn: *Acta Met.*, 5 (1957) 168
- [39] H.I. Aronson, K.C. Russell, and G.W. Lorimer: *Met. Trans.* 8A (1977) 1644
- [40] A.R. Jones and B. Ralph: *Acta Met.*: 23 (1975) 355
- [41] H.B. Aaron, D. Fainstein and G.R. Kotler: *J. Appl. Phys.* 41 (1970) 4404
- [42] M. Dahlen and L. Winberg: *Acta Met.* 28 (1980) 41
- [43] J.V. Bee, A.R. Jones and P.R. Howell: *J. Mater. Sci.* 15 (1980) 337
- [44] D.E. Stephens and G.R. Purdy: *Acta Met.*, 23 (1975) 1343
- [45] J.V. Bee, A.R. Jones and P.R. Howell: *J. Mater. Sci.*, 15 (1980) 337
- [46] J.V. Bee, A.R. Jones and P.R. Howell: in *Recrystallization and Grain Growth of Multiphase and Particle Containing Materials*, ed. N. Hansen et al., Riso National Laboratory, Roskilde, Denmark (1980) 153
- [47] P.R. Howell and J.V. Bee: in *Recrystallization and Grain Growth of Multiphase and Particle Containing Materials*, ed. N. Hansen et al., Riso National Laboratory, Roskilde, Denmark (1980) 171
- [48] A.P. Rama Mohan, P. Rama, and T.R. Anantharaman: *Trans. Indian Inst. Met.*, 18 (1965) 173

- [49] S. Matsuo and L.M. Clarebrough: Acta Met. 11 (1963) 1195
- [50] H. Suzuki: J. Phys. Soc. Japan, 17 (1962) 322
- [51] M. Bouchard and C. Thomas: Acta Met. 23 (1975) 1485
- [52] P.G. Boswell and G.A. Chadwick: J. Mater. Sci. 12 (1977) 1879
- [53] H.E. Cook and J.E. Hilliard: Trans. AIME 233 (1967) 142
- [54] J. Dutkiewicz: Bull. Acad. Pol. Sci. Ser. Sci. Tech., 22 (1974) 323
- [55] J.W. Cahn: Trans. AIME 242 (1968) 166
- [56] H.O. Asbeck: Doctoral Dissertation, RWTH Aachen (1973)
- [57] F. Haessner, G. Hoschek and G. Tölg: Acta Met. 27 (1979) 1539
- [58] F. Haessner and W. Hemmirger: Z. Metallk. 69 (1978) 553
- [59] P.G. Schewmon: in *Diffusion in Solids*, J. Williams and O.K. Jenks (1983) 111
- [60] K.H. Virnich: Doctoral Dissertation, RWTH Aachen (1979)



MICHIGAN STATE UNIV. LIBRARIES



31293005902527